***Bacteroides intestinalis*–Driven Arabinoxylan Fermentation Mitigates Inflammatory and Metabolic Dysfunction**

Ziyu Zhou[1,9], Ka Lam Nguyen[1,9], Sijie Chen[1,9], Yuexi Wang[1], Min Li[1], David Biachi[2], Weihao Ge[2], Shanny Kuo[3], Salwa Gharieb[1], Emily Tung[1], Ronak Parmar[1], Jie Ji[1], Rohit Khorana[1], Ahmed Hetta[4,5], Isaac Cann[4,5], Roderick Mackie[4,5], Gee Lau[3,5,7], Jing Yang[1], Wenyan Mei[1,5,6,7,8,] *

1 Department of Comparative Biosciences, University of Illinois Urbana-Champaign, Urbana, Illinois
2 National Center for Supercomputing Applications, University of Illinois Urbana-Champaign, Urbana, Illinois
3 Department of Pathobiology, University of Illinois Urbana-Champaign, Urbana, Illinois
4 Department of Animal Sciences, University of Illinois Urbana-Champaign, Urbana, Illinois
5 Carl R. Woese Institute for Genomic Biology, University of Illinois Urbana-Champaign, Urbana, Illinois
6 Division of Nutritional Sciences, University of Illinois Urbana-Champaign, Urbana, Illinois
7 Cancer Center at Illinois, University of Illinois Urbana-Champaign, Urbana, Illinois
8 Personalized Nutrition Initiative, University of Illinois Urbana-Champaign, Urbana, Illinois
9 These authors contributed equally to the work.
10 Lead contact

Summary

Insufficient dietary fiber intake is strongly associated with gut microbiome dysfunction and an increased risk of noncommunicable diseases. Synergistic synbiotics, which pair defined microbial strains with their preferred carbohydrate substrates, offer a promising strategy to restore these functions. However, the rational design of such interventions remains challenging by insufficient understanding of microbial fiber-degrading capacities and the host-relevant bioactivities of fermentation-derived metabolites. Here, we identify human colonic commensal *Bacteroides intestinalis* (*B. intestinalis*) as a key microbial mediator of dietary fiber-driven metabolic, immune, and neuronal benefits. We demonstrate that the synergistic interaction between *B. intestinalis* and its preferred substrate, insoluble wheat arabinoxylan abundant in dietary fiber, enhances the production of anti-diabetic and anti-steatotic bile acid species, hyocholic acid and hyodeoxycholic acid, anti-inflammatory, antioxidant phenolic compounds, and a spectrum of neuroactive compounds. These metabolic effects are accompanied by coordinated transcriptional remodeling in the colon and spleen implicating pathways governing circadian rhythm regulation, lipid metabolism, and immune defense. Importantly, these beneficial effects are preserved in conventionally raised mice with established high fat diet-induced obesity, where BI and inWAX improve glucose tolerance. Our findings uncover a mechanistic framework linking *B. intestinalis*-mediated fiber fermentation to gut–liver–brain crosstalk and establish a rational foundation for precision synbiotic design.

Introduction

The global adoption of a low-fiber Western diet has fundamentally altered gut microbiota function, contributing to the escalating burden of noncommunicable metabolic and inflammatory diseases worldwide. In contrast, higher dietary fiber intake is linked to increased gut microbiome diversity and reduced risk of inflammatory and metabolic diseases [1]. Dietary fiber has been shown to lowers cholesterol, improve glucose homeostasis and weight control, and reduce the risk of colorectal cancer. Emerging evidence further implicates dietary fiber in supporting cognitive function [2-4]. These important observations underscore the therapeutic potential of dietary fiber in preventing and managing noncommunicable diseases. Yet, fiber-deficient Western diet has limited the daily consumption of fiber and caused the loss or reduction of many fiber-fermenting microbes in gut microbiota, thereby diminishing the benefits conferred by dietary fiber. This has spurred interest in microbiome-targeted interventions using dietary fibers (prebiotics), fiber-fermenting microbes (probiotics), and their combinations. In particular, synergistic synbiotics, which pair defined microbial strains with their preferred carbohydrate substrates, offer a compelling strategy to enhance engraftment, persistence, and functional output of beneficial microbes in the gut. Despite this promise, the rational design of synbiotic interventions remains constrained by a lack of understanding of microbial fiber-degrading repertoires, substrate specificities, and the host-relevant bioactivities of fermentation-derived metabolites.

The benefits of dietary fiber stem not only from its physicochemical properties but also from bioactive metabolites produced during its fermentation by gut commensal bacteria. Short-chain fatty acids (SCFAs) represent the most well-studied class of fiber-derived metabolites and exert broad benefits on immunity, intestinal barrier integrity, and metabolic homeostasis [5-8]. Emerging findings, however, suggest that many health-promoting effects of dietary fiber may be attributed to microbial metabolites other than SCFAs [9]. For instance, dietary fiber intake has been reported to increase the production of aromatic amino acid derivatives, neurotransmitters, secondary bile acids, and B vitamins [9]. These findings highlight the critical need to identify the gut microbes that produce these metabolites, the specific dietary substrates they preferentially ferment, and the mechanisms by which these metabolites influence host physiology. Addressing this gap is essential for fully harnessing the therapeutic potential of gut microbe–mediated fiber fermentation.

Here, we identify *Bacteroides intestinalis* (hereafter BI) as a key microbial mediator of dietary fiber–driven metabolic, immune, and neuronal benefits. We show that BI ferments insoluble wheat arabinoxylan (inWAX) *in vivo*, eliciting systemic and intestinal effects that collectively ameliorate inflammatory and metabolic disease phenotypes. BI is a member of fiber-degrading *Bacteroides* spp. of the phylum Bacteroidetes, a major group of bacteria in the human adult distal gut. It was originally isolated from a healthy Japanese individual. Our prior *in vitro* work demonstrated that BI harbors esterase gene-enriched polysaccharide utilization loci (EGE-PULs) capable of sensing and degrading inWAX to release ferulic acid, a phenolic compound with potent anti-inflammatory and antioxidant properties [10]. Arabinoxylan is a major plant cell wall polysaccharide abundant in cereals such as wheat, barley, and oats [11]. It consists of a β1-4-linked xylose backbone decorated with arabinose side chains that is esterified to hydroxycinnamic acids, including ferulic and *p*-coumaric acids. [12]

We demonstrate that BI-mediated inWAX fermentation *in vivo* elevates systemic levels of phenolic compounds and bile acids with anti-inflammatory, antioxidant, and anti-diabetic

activities. Concomitantly, it activates intestinal gene programs governing triglyceride metabolism and circadian rhythm regulation. Functionally, mice receiving the BI-inWAX synbiotic display enhanced resistance to dextran sulfate sodium (DSS)-induced colitis, a major type of inflammatory bowel diseases (IBD). This accompanied by upregulation of genes that protect intestinal barrier function and improve spleen immune responses, suggesting a coordinated local and systemic immune defense. In the context of high-fat diet (HFD)–induced obesity, BI and inWAX enhanced gut microbial biotransformation of plant-derived polyphenols into anti-inflammatory and antioxidant phenolic compounds. In parallel, this synbiotic selectively expands bile acid species (HCA and HDCA) with anti-diabetic and hepatoprotective activities. This is accompanied by improved glucose tolerance. Notably, this intervention also increases the abundance of neurotransmitter-related amino acids.

Collectively, our findings establish BI-mediated inWAX fermentation as a mechanistically defined synbiotic that integrates microbial metabolism with host metabolic, immune, and neuronal pathways**.** This work provides both a conceptual framework and experimental foundation for the rational design of next generation synbiotics to prevent and treat noncommunicable diseases.

Results

BI promoted colon mucus layer formation

To determine the physiological impact of BI, we inoculated viable BI and heat-killed BI to germ-free GF) mice fed a chow diet (Fig 1A). Control mice were inoculated with vehicle (culture medium). By comparing mouse physiological responses to viable versus heat-killed BI, we can differentiate the physiological impacts mediated by BI-derived metabolites, as heat-killed bacteria are unable to produce them. Viable BI significantly reduced the cecum size and weight when compared to the vehicle control and heat-killed BI but had no effect on body weight and intestine lengths (Fig 1B, Fig S1). Both viable BI and heat-killed BI significantly increased the percentages of goblet cells in the colon, duodenum, and ileum but not in the jejunum when compared to the vehicle control (Fig 1C and Fig S1). Notably, viable BI induced a greater increase in the number of goblet cells than heat-killed BI in the colon (Fig 1D). However, only mice inoculated with viable BI developed a substantially thicker mucus layer in the colon (Fig 1D). These findings suggest that both *BI* cell wall components and metabolites promote region-specific goblet cell differentiation, whereas mucus secretion is selectively stimulated by *BI*-derived metabolites.

BI-mediated fermentation of inWAX increased systemic level of ferulic acid

We next examined BI's capability and capacity of fermenting INWAX and releasing ferulic acid *in vivo*. GF mice were inoculated with viable BI or vehicle and fed a customized diet containing 5%, 10%, or 15% inWAX, or a control diet in which inWAX was replaced with 15% cellulose (Fig 2A). Cellulose was used a control for non-specific fiber effect because BI lacks the enzymatic capacity to degrade it.[10]. Systemic ferulic acid levels in mouse serum were measured with the LC-MS/MS. As shown in Fig 2B, inWAX increased circulating ferulic acid levels in a dose-dependent manner. No significant increase in ferulic acid was observed when inWAX was increased from 10% to 15%, suggesting that 10% inWAX may represent a dose close to the saturation point of BI's fermentation capacity. These results demonstrate that BI can ferment inWAX *in vivo* to release ferulic acid and elevate its systemic level, highlight its anti-inflammatory and antioxidant potential.

BI-mediated fermentation of inWAX generated disease-protecting blood metabolome

To unbiasedly evaluate the impact of BI-mediated fermentation of inWAX on host metabolism, we performed an untargeted metabolomics analysis using serum samples from BI-inoculated mice fed 15% inWAX or 15% cellulose. Mice receiving inWAX diet showed a very distinct circulating metabolic profile from those receiving cellulose (Fig 2C), indicating that BI-mediated fermentation of inWAX shifts host metabolism. 22 known metabolites were significantly elevated by inWAX (Fig 2D, Supplemental Table 1). Among them, ferulic acid is one of the most elevated metabolites, which is consistent with the observation from ferulic acid measurement. In addition to ferulic acid, two additional phenolic acids that have antioxidant and anti-inflammatory properties, M-coumaric acid and syringic acid, are also increased (Fig 2D and 2E). This is accompanied by an elevated ratio of reduced glutathione (GSH) to oxidized glutathione (GSSG) (Fig 2F), a hallmark of improved cellular health and redox balance. This finding indicates that BI-mediated fermentation of inWAX improved the antioxidant and anti-inflammatory capability of host.

Of note, four of the six most elevated metabolites in inWAX-fed mice are bile acids, including cholic acid (CA), taurocholic acid (TCA), tauroursodeoxycholic acid (TUDCA), and hyocholic acid (HCA) (Fig 2D and 2E). Both TUDCA and HCA are anti-diabetic and can improve glucose homeostasis [13,14] [15,16]. Although the increase of TUDCA did not reach statistical significance due to large inter-individual variability and small sample size, the consistent upward trend supports a biological effect.

The metabolite that showed the highest increase in inWAX-fed mice is D,L-N,N-didesmethyl-o-desmethylvenlafaxine, a derivative of venlafaxine. Venlafaxine is a serotonin-norepinephrine reuptake inhibitor and has been clinically used for treating depression and anxiety. The elevation of this compound suggests the presence of an as-yet-uncharacterized venlafaxine-like metabolite derived from BI-mediated inWAX fermentation or host metabolism.

23 known metabolites are decreased in inWAX-treated mice (Supplemental Table 2). Intriguingly, more than 56% of them are involved in lipid metabolism., including 7 derivatives of carnitine and 6 members of lysophosphatidylcholines (LPCs) (Fig 2G). Derivatives of carnitine act as a transport system to move activated fatty acids into mitochondria for β-oxidation, which is a primary energy-generating process. LPCs are bioactive signaling molecules derived from the partial hydrolysis of phosphatidylcholines and are involved in lipid signaling and cell membrane remodeling. The decreased circulating levels of these metabolites is presumably an indicative of improved lipid metabolism and energy homeostasis through a gut-liver-metabolism axis.

Together, these findings demonstrate that supplementation with BI and inWAX elevates systemic levels of phenolic compounds and bile acids with anti-inflammatory, antioxidant, and anti-diabetic activities, improved cellular redox balance, and reshaped lipid metabolism.

BI-mediated inWAX fermentation shifted the colonic transcriptome

Given that colon is directly exposed to microbial metabolites, we next assessed the effect of BI-mediated inWAX fermentation on colon transcriptome. 15% inWAX-treated mice exhibited 15 upregulated genes in the colon when compared to 15% cellulose-fed mice (Fig 3A, Supplementary

Table 2). Strikingly, the gene that is mostly upregulated is *cyclic AMP responsive element–binding protein 3–like 3*(*Creb3l3*), a transcriptional factor that promotes triglyceride metabolism. Loss-of-function *Creb3l3* variants in humans have been associated with hypertriglyceridemia, whereas overexpression of *Creb3l3* reduces arteriosclerotic lesions in mouse models of arteriosclerosis [17-20]. Thus, an elevation of *Creb3l3* underscores the potential of BI and inWAX in protecting against hypertriglyceridemia and arteriosclerosis.

Surprisingly, 5 of the 15 increased genes are core regulators of circadian rhythms (Fig 3A). *Per1*, *Per2,* and *Ciart* (also called *Chrono*) are key components of a negative feedback loop in the circadian control by inhibiting the activity of the CLOCK–BMAL1 complex, the master transcriptional activator of clock genes, whereas *Dbp and Tef* are circadian clock-controlled transcription factors in the PAR bZip family that mediate circadian clock output pathways via D-box elements (Fig 3B) [21-23]. Using quantitative real-time PCR, we validated the increased expression of these genes in the colons of inWAX-treated mice (Fig 3C).

Other upregulated genes include *Hmox1*, *Fkbp5,* and *Hif3a* that respond to stress and hypoxia [24-26], *Slc2a5* and *Abcc2* for membrane transport[27,28], *Kyat1* for the tryptophan Kynurenine Pathway, and *Tsku* and *Lefty1* for tissue development and homeostasis [29,30].

Only two genes were downregulated in inWAX-treated mice, including *Pou1f1*, a transcriptional factor with unknown intestinal function, and *Tac1*, which encodes the precursor for neuropeptides tachykinins that regulate intestinal motility, secretion, and vascular functions (Fig 3A).

Together, these findings indicate that BI-mediated fermentation of inWAX influences intestinal function at least in part by activating genes essential for triglyceride metabolism and intestinal circadian clock.

BI-mediated inWAX fermentation protects against colitis

Given that BI-mediated fermentation increased systemic level of anti-inflammatory and antioxidant metabolites, we investigated its protective effect against IBD. BI mono-associated male mice received 15% inWAX or 15% cellulose were challenged with 2% DSS for 5 days to induce colitis, a major type of IBD (Fig 4A, thereafter inWAX:DSS+ and Cellu;DSS+, respectively). Mice treated with 15% inWAX without DSS was used as a control (inWAX;DSS-). InWAX:DSS+ mice exhibited significantly less body weight loss in response to DSS treatment when compared to Cellu;DSS+ mice (Fig 4B). At the end of the treatment, Cellu:DSS+ mice showed a markedly increase in the spleen size because of inflammation. This splenomegaly was substantially attenuated in inWAX;DSS+ mice (Fig. 4C), suggesting reduced systemic inflammation. Consistently, inWAX:DSS+ mice displayed significantly lower colonic histopathological scores, characterized by reduced crypt dilation, fibrosis, and inflammatory infiltrates (Fig. 4D).

Collectively, these results strongly indicate that BI-mediated fermentation of inWAX confers protection against DSS-induced colitis.

inWAX fermentation induced protective colon transcriptome against DSS

To elucidate the molecular basis of colitis resistance conferred by BI and inWAX, we analyzed DSS-induced transcriptional changes in the colon. Relative to Cellu;DSS+ mice, inWAX;DSS+ mice exhibited upregulation of 45 genes (Fig. 5A; Supplemental Table 3). This includes 7 genes involved in innate immune defense (*Reg3b*, Retn, Apol7c, Cd177, Clec14a, Clec2e, Mafb). *Reg3b* was among the most strongly induced genes, and it encodes an antimicrobial lectin that limits bacterial translocation and protects against DSS-induced colitis [31-33], suggesting enhanced host defense to DSS-induced colitis.

Unexpectedly, inWAX treatment also induced a set of genes classically associated with male fertility, including *Svs2*, *Ddx3y*, *Uty* (*Kdm6c*), *Kdm5d*, *Eif2s3y*, and *Uba1y*. Five of these genes are Y chromosome-linked and function in RNA translation (*Eif2s3y*, *Ddx3y*), epigenetic regulation (*Kdm6c*, *Kdm5d*), and protein ubiquitination (*Uba1y*) [34-38]. *Svs2* is a non–Y-linked gene encoding a secreted seminal vesicle protein that protects sperm from immune attack[39], with an unknown role in the intestine. This interesting finding suggests that BI-mediated inWAX fermentation induces sex-based immune modulation in the colon in response to DSS insult.

Strikingly, nearly half of the upregulated genes encoded metabolic regulators involved in lipid, protein, carbohydrate, and xenobiotic metabolism (Fig 5C and 5D). Most of them encode enzymes or regulators of enzymes, underscoring a broad metabolic reprogramming of the colon. Among them, lipid metabolic pathways show the strongest enrichment (Fig 5B and 5C), spanning multiple layers of lipid metabolism regulation, including lipid synthesis and desaturation (*Thrsp*, *Scd1*), storage (*Plin1*), hydrolysis and mobilization (*Apoc2*, *Angptl4*, *Ces1f*, *Ces1g*), and extracellular regulation of lipid metabolic signaling (*Tsku*), which highlighted a coordinated lipid metabolic reprogramming in the colon. Notably, *Tsku* was also upregulated in inWAX-treated mice without DSS treatment (Supplemental Table 2).

Importantly, many of these metabolism regulatory genes possess immune-regulatory functions. For instance, *Scd1* encodes Stearoyl-CoA desaturase-1 to convert saturated fatty acids into monounsaturated fatty acids [40], and can attenuate DSS-induced colitis [41]. *Ido1* modulates immune responses by catabolizing tryptophan[42] [43] [44]. *Mcpt1* encodes a Mast cell protease that is predominantly expressed in intestinal mucosal mast cells and have multifaced roles in inflammation [45]. *Arg2* encodes a mitochondrial enzyme involved in arginine metabolism and nitric oxide synthesis, and can influence immune cell function and suppress inflammation [46-48] [49]. *Vnn1*, encoding a pantetheinase that converts pantetheine to pantothenate and cysteamine, enhances SCFA production and protect against DSS-induced colitis[50]. *Angptl4* represses lipoprotein lipase and is also immune regulatory [51].

Collectively, these data indicate that BI-mediated fermentation of inWAX induces a coordinated transcriptional program that couples metabolic reprogramming with enhanced mucosal immune protection. This reveals a central role for gut microbiota-driven metabolic remodeling in promoting intestinal resilience to inflammatory injury.

Consistent with attenuated inflammatory stress in inWAX-treated mice, we observed significant downregulation of genes associated with wound healing, stress responses, and cell junction assembly, along with with reduced activities in MAPK signaling and PI3K-AKT signaling (Fig. 5D, Supplemental Table 3).

inWAX fermentation induced protective spleen architecture and transcriptome against DSS
The spleen is a major secondary lymphoid organ that integrates hematopoietic and immunological functions. Given our observation that BI and inWAX markedly attenuated DSS-induced splenomegaly, we next examined the impact of BI-mediated inWAX fermentation on splenic architecture and transcriptional programs. Compared with cellulose-treated controls, inWAX-treated mice exhibited a pronounced expansion of the white pulp (Fig 6A), the lymphocyte-enriched compartment of the spleen, indicative of enhanced adaptive immune cell abundance. This was confirmed by transcriptome profiling, which showed broad activation of genes essential for B and T cell proliferation, differentiation and activation, immunoglobulin production, and cytokine signaling (Fig 6B). Positive innate immune response is also upregulated. This is accompanied by signaling pathways of Th1 and Th2, Th17 cell differentiation and JAK-STAT. In contrast, genes suppressed by inWAX treatment were enriched for DNA replication and cell cycle pathways (Fig 6C), which presumably attenuated splenomegaly.

To define how these transcriptional changes translate into immune cell composition, we performed immune cell fraction analysis. InWAX-treated mice showed a robust expansion of adaptive immune populations, including B cells, T cells. Macrophages also had considerable expansion, although to a less extent compared to lymphocytes. Only a slight increase of natural killer cells was observed (Fig 6D and 6E). In contrast, dendritic cells were reduced in inWAX-treated mouse spleen, suggesting dampened activation of pro-inflammatory innate immune circuits.

Notably, 16 genes induced in the spleen were also upregulated in the colon of inWAX-treated mice (Fig 6F). These shared genes included four Y-linked genes (*Ddx3y, Eif2s3y, Kdm5d,* and *Kdm6c*), seven metabolic enzymes or regulators, the fructose transporter *Slc2a5*, the stem cell-associated factor *Piwil4*, and immune-related genes (*Apol7c* and *Retn*). This overlap suggests that BI-mediated inWAX fermentation activates a conserved transcriptional program in both the intestine and spleen to counteract DSS-induced inflammatory stress, revealing coordinated immune–metabolic reprogramming across local and systemic compartments. The induction of Y-linked genes in both the colon and spleen suggests a potential sex-based response to inflammatory stress.

Together, these findings demonstrate that BI-mediated inWAX fermentation alleviates DSS-induced systemic inflammation by primarily expanding lymphocytes to promote a protective adaptive immune state.

InWAX fermentation ameliorates HFD-induced metabolic dysfunction
Given that BI-mediated inWAX fermentation increased systemic levels of metabolites that have anti-inflammatory, antioxidant, and anti-diabetic properties, and reprogrammed the intestine and spleen transcriptome to enhance protection against DSS-induced inflammatory stress, we next examined whether these beneficial effects can be preserved in the context of HFD-induced gut dysbiosis to ameliorate metabolic dysfunction in obesity. Because BI is not a native resident of C57B6 black mice (Fig 7B), we used B6 mice for the study. As outlined in Fig. 7A, conventionally raised male mice were first preconditioned on HFD to induce obesity and then randomly assigned to receive HFD alone (HFD), HFD supplemented with 10% cellulose (HFD+Cellu), or HFD supplemented with 10% inWAX (HFD+inWAX). As in BI mono-association experiments, cellulose served as a non-fermentable fiber control to distinguish inWAX-specific effects from nonspecific fiber effects. After a 5-day dietary acclimation period, mice in all three groups were

orally inoculated with BI every other day for four weeks. BI was administered to the HFD and cellulose groups to control for BI-induced effects independent of fermenting inWAX. Body weight was monitored every other day during the first 12 days of treatment. While there is no significant difference in the weight gain between HFD+inWAX and HFD+Cellu mice, mice in these two groups consistently gained less weight than HFD-only control, likely reflecting reduced caloric intake associated with fiber supplementation (Fig S2).

Glucose tolerance was assessed on day 29. HFD+inWAX mice displayed a consistent lower blood glucose level at 30-, 60-, and 90-minutes following glucose administration compared with both HFD-only and HFD+Cellu groups, with the difference between HFD and HFD+inWAX groups at 60 minutes reaching statistical significance (Fig. 7C). While cellulose-treated mice exhibited modest reductions in glucose levels relative to HFD controls, they are not statistically significant, suggesting a limited, nonspecific fiber effect. These results indicate an improvement in glucose tolerance delivered by the synergistic function of BI and WAX.

InWAX fermentation induced health-promoting bile acid species

To determine the metabolic basis of inWAX fermentation-conferred health benefits in obese mice, we evaluated its impact on bile acid pool. InWAX-treated mice had a markedly increase in the levels of four bile acid species (Fig 7D). This includes HCA, hyodeoxycholic acid (HDCA), omega-muricholic acid (ωMCA) and Deoxycholic Acid (DCA). Interestingly, except for HCA, the synthesis of which is still unclear in mice, the remaining are secondary bile acids generated by microbial biotransformation. In mice, HDCA can be generated through microbial 7-dehydroxylation and 6-hydroxy epimerization of muricholic acids (MCA) [52,53], which constitute major primary bile acids in mice. HDCA is also reported to be transformed from HCA through microbial 7α-dehydroxylation of HCA[53]. ωMCA is produced through a two-step microbial epimerization where bacteria first oxidize the 6β-hydroxyl group of beta-Muricholic acid (β-MCA) to a 6-oxo intermediate, which is then reduced to a 6α-hydroxyl group. DCA is transformed from CA through a multi-step microbial 7α-dehydroxylation process. We then checked the level of their precursors. In inWAX-treated mice, the levels of αMCA showed an increased trend but not statistically significant while the levels of βMCA and CA are not markedly increased, suggesting that the increase of HDCA and ωMCA from these precursors are predominantly due to enhanced microbial transformation rather than the increased availability of their precursors.

Notably, HCA was also induced by inWAX but not cellulose in BI mono-associated mice (Fig. 2D), indicating that metabolites from BI-mediated inWAX fermentation can promote HCA production through hepatic pathways. Notably, both HCA and HDCA have been reported to improve glucose homeostasis in mouse models of diabetes, and HDCA is also capable of ameliorating atherosclerosis and non-alcoholic fatty liver disease (NAFLD) [54-56]. The serum levels of HCA and HDCA are lower in people with obesity, type 2 diabetes and metabolic dysfunction-associated steatotic liver disease. The selective expansion of these selectively expands anti-diabetic and anti-steatotic bile acid species health-promoting bile acid species underscores the therapeutic potential of BI and inWAX in preventing and mitigating obesity-associated metabolic dysfunction.

InWAX fermentation induced the fecal metabolome shift

We next used untargeted fecal metabolomics analysis to unbiasedly examine the impact of inWAX and BI on the fecal metabolome, a functional readout of microbial metabolic activity. We observed a marked remodeling of the fecal metabolic landscape in inWAX-treated mice compared with both HFD and cellulose-treated controls (Fig. 8A). In total, 123 metabolites were uniquely altered by inWAX, with 85 increased and 38 decreased (Fig. 8B; Supplemental Table 5), defining a distinct microbial metabolic signature induced by BI and inWAX under HFD conditions.

The metabolites exclusively upregulated by inWAX were highly enriched for amino acids and peptides (47%) (Fig 8C, Supplemental Table 6). Strikingly, ~33% of them belonged to neurotransmitters and their precursors (Fig 8D), suggesting that BI and inWAX may shift protein metabolism toward enhanced neuroactive compound production and potentially strengthen the gut-brain metabolic crosstalk. The second most enriched class comprised fatty acid derivatives, predominantly oxygenated fatty acids (oxylipins) derived from long-chain polyunsaturated fatty acids (Supplemental Table 6), consistent with the role of this synbiotic in rewiring lipid metabolic pathways.

In line with BI-mediated liberation of ferulic acid from inWAX, we observed a robust increase in ferulate and its derivative dihydroisoferulic acid. In addition, six other phenolic compounds were significantly elevated, including simple phenolics (o-coumaric acid and 3,4-dihydroxyacetophenone), flavonoids (7-O-methyleriodictyol and jaceoside), and enterolignans (enterolactone and enterodiol) (Fig. 8E). These bioactive compounds are microbial fermentation products of dietary polyphenols and are well documented for their anti-inflammatory and antioxidant activities [57,58,59]. In parallel, four complex plant polyphenols (syringaresinol, 6H-Benzofuro[2-c]benzopyran, picropodophyllin, methyl trans-cinnamate) are decreased. Syringaresinol can be microbially converted to enterolactone and enterodiol.[60] the upregulated lignans and flavonoids. This finding indicates enhanced microbial biotransformation of dietary polyphenols into bioactive metabolites.

Additionally, inWAX fermentation significantly elevated nicotinic acid (vitamin B3) and pantothenate (vitamin B5) (Fig. 8E), two essential cofactors for cellular energy metabolism. While nicotinic acid can be synthesized by both host and microbes, pantothenate is exclusively produced by gut microbes, further supporting a microbiota-dependent reprogramming of host metabolic capacity.

Unlike upregulated metabolites, the metabolites exclusively downregulated in InWAX-treated mice were structurally heterogeneous (Supplemental Table 6). Besides four aforementioned plant polyphenols, it includes sphingolipids and glycerophospholipids, suggesting a role of BI and inWAX in modulating lipid metabolism.

We also identified 49 metabolites altered in both inWAX- and cellulose-treated mice (35 increased, 14 decreased), likely reflecting shared fiber-dependent effects. Most of the co-upregulated metabolites are amino acids and short peptides, indicating that both fermentable and nonfermentable dietary fiber enhanced protein metabolism. Interestingly, the co-downregulated metabolites include 6 phosphatidylcholine derivatives involved in membrane composition regulation and lipid mediator signaling pathways. Notably, 3 of them, LysoPC(17:0), LPC(16:0), LysoPC (16:0), are also downregulated in the serum of inWAX-treated BI mono-associated mice,

suggesting that BI-mediated inWAX fermentation has a direct role in reducing their production, and this function is preserved under the gut microbiota of HFD-induced obesity.

Adddtionally, 49 metabolites were uniquely altered by cellulose, with 17 increased and 32 decreased, indicating that fermentable inWAX and non-fermentable cellulose exert distinct metabolic effects under high-fat diet conditions. Notably, 8 of the 17 cellulose-upregulated metabolites were short peptides, suggesting that, despite being non-fermentable, cellulose may still influence protein metabolism, albeit through pathways distinct from those activated by fermentable inWAX. With the exception of a single sulfated dietary polyphenol metabolite (3-(3-hydroxyphenyl)propionic acid sulfate), cellulose did not increase HCA, HDCA, or the beneficial phenolic compounds observed in inWAX-treated mice. These findings underscore that the synergistic interaction between BI and inWAX is critical for conferring the robust health-promoting effects.

Altogether, by testing BI-inWAX effect in BI-monoassociated mice and conventionally raised mice with HFD-induced obesity, we demonstrate that the synergistic interaction between *BI* and its preferred fiber substrate, inWAX, enhances microbial production of anti-inflammatory and antioxidant phenolic metabolites and selectively expands anti-diabetic and anti-steatotic bile acid species. These changes are accompanied by coordinated transcriptional remodeling in the colon and spleen, implicating pathways involved in circadian regulation, lipid metabolism, and immune homeostasis. Importantly, these beneficial effects are preserved in conventionally raised mice with established HFD-induced obesity, where BI and inWAX significantly improves glucose tolerance. These findings provide a strong rationale that this synbiotic retains its health-promoting capacity under obese conditions and may represent a powerful strategy to improve metabolic homeostasis in people with obesity.

Discussion

Insufficient dietary fiber intake is strongly associated with gut microbiome dysfunction and an increased risk of noncommunicable diseases, particularly inflammatory and metabolic disorders, which together impose a growing global health and economic burden[1]. Dietary fiber improves cholesterol metabolism, glucose homeostasis, body weight regulation, and cognitive function[2-4], highlighting its broad therapeutic potential. However, modern low-fiber diets have driven the loss or depletion of fiber-fermenting microbes, thereby attenuating the health benefits of fiber consumption. Synergistic synbiotics, which pair defined microbial strains with their preferred carbohydrate substrates, offer a promising strategy to restore these functions. Nevertheless, the rational design of such interventions is constrained by insufficient understanding of microbial fiber-degrading capacities and the host-relevant bioactivities of fermentation-derived metabolites.

In this study, we present compelling evidence that BI is a key microbial mediator of dietary fiber-driven metabolic, immune, and neuronal benefits. We show that the synergistic interaction between BI and its dietary fiber substrate, inWAX, selectively enhances the production of anti-inflammatory, antioxidant, and anti-diabetic phenolic compounds and bile acid species, even under the context of HFD-induced gut microbiota. Further it remodels protein metabolism toward enhanced neuroactive compound production, which potentially strengthen the gut–brain metabolic crosstalk. These microbial metabolites are accompanied by coordinated transcriptional

reprogramming in the colon and spleen that improves circadian rhythm regulation, lipid metabolism, and immune defense.

A particularly notable finding is the selective expansion of health-promoting bile acids, such as HCA, HDCA, and TUDCA. These bile acids have been shown to ameliorate metabolic disorders such as diabetes, atherosclerosis, and non-alcoholic fatty liver disease (NAFLD) [15 54-56]. Reduced systemic levels of HCA and HDCA in individuals with obesity and diabetes further underscore their therapeutic relevance [15,16] TUDCA, which is clinically approved for primary biliary cholangitis due to its cytoprotective properties, has also shown promise in obesity, IBD, and neurodegenerative diseases [13,14,61-65]. The selective expansion of these beneficial bile acids by BI and inWAX, even under HFD-induced obesity, highlights the translational potential of this synbiotic strategy for metabolic disease intervention.

Mechanistically, how BI-mediated inWAX fermentation enhances the production of these bile acid species is of great interest. In BI mono-associated mice, inWAX increased systemic TUDCA and HCA levels compared with cellulose, suggesting that BI induced TUDCA and HCA through fermenting inWAX, e.g., by releasing metabolites that enhances their production, rather than producing enzymes. This effect likely arises from fermentation-derived metabolites that reprogram bile acid synthesis or biotransformation pathways in the liver, a mechanism that warrants further investigation

In HFD-treated conventionally mice, BI and inWAX increase the production of HCA, HDCA, ωMCA, and DCA. In mice, HDCA and ωMCA can be biotransformed from αMCA and βMCA by gut microbes through epimerization and dehydroxylation. Because αMCA and βMCA levels were not markedly altered by inWAX in these mice, the elevated abundance of these secondary bile acids is likely attributable to enhanced microbial conversion rather than increased availability of these precursors. Notably, a study in rat found that an unidentified Gram-positive microbe Termed HDCA-1 can convert βMCA or HCA to HDCA. The strain HDCA-1 could only do this conversion in the presence of a bile acid-deconjugating strain and a growth factor-producing *R. productus* strain in germ free rats, highlighting a microbial community effect in producing HDCA[53]. Moreover, a recent study shows that *Bacteroides ovatus*, a member of *Bacteroides* spp., can enhance HDCA production by supporting the growth of *Clostridium scindens* [66], suggesting that cross-feeding based HDCA produciton mechanism. It is, thus, likely that the synergistic interaction of BI and inWAX may provide nutrients that cross feed members in such a biotransformation community to enhance its activity.

In addition to selectively expanding beneficial bile acid species in HFD-induced obese mice, BI and inWAX also enhance the microbial biotransformation of dietary plant polyphenols into a spectrum of bioactive metabolites, including simple phenolics, flavonoids, and enterolignans. These compounds are well documented for their potent anti-inflammatory and antioxidant activities[57,58,59]. This enhanced biotransformation suggests that BI and inWAX not only generate specific metabolites with direct therapeutic potential, such as ferulic acid, but also broadly augment gut microbiota–mediated metabolic processes. As a result, this synbiotic intervention substantially amplifies the host's capacity to extract and utilize the health-promoting benefits of dietary fiber.

An unexpected and conceptually important finding is the induction of core circadian clock genes in the intestine following BI-mediated inWAX fermentation. The intestinal circadian clock is critical for mucosal barrier integrity, immune responses, metabolism, and gut microbiota function. Disrupted circadian rhythm has been associated with a higher risk and more aggressive course of IBD [67,68]. Reduced colonic expression of *Per1* and *Per2* has been observed in patients with IBD [69,70], and mice lacking these genes exhibit impaired antimicrobial secretion and heightened sensitivity to DSS-induced colitis [71]. Our findings uncover a previously unrecognized link between microbial fiber fermentation and intestinal circadian regulation, potentially connecting microbial metabolism with gut–brain–immune axis signaling.

Another interesting finding from this study is inWAX fermentation-induced robust activation of Y-linked genes, *Ddx3y, Eif2s3y, Kdm5d,* and *Kdm6c,* in both the colon and spleen during immune defense against DSS-induced colitis. These genes function in RNA translation and epigenetic regulation, processes essential for stress and immune responses. Their induction suggests a potential sex-biased component in the host response to fiber fermentation. Future studies examining whether BI and inWAX similarly regulate the corresponding X-linked counterparts of these genes in female mice will be essential to clarify this dimension of synbiotic responsiveness.

Together, our findings expand the prevailing paradigm of fiber-microbiota-host interactions by demonstrating that dietary fiber-driven health benefits can be mediated by microbial metabolites beyond SCFAs. Importantly, our work establishes a rational framework for the design of synergistic synbiotics, which pairs defined microbial strains with specific fiber substrates to target inflammatory and metabolic diseases. This study integrates multi-omics approaches with mono-associated gnotobiotic mouse models and conventionally raised high-fat diet-induced obese mice, which provides a comprehensive and mechanistic evaluation of host–microbe–diet interactions.

Limitation of the study

One limitation of this study is the absence of a direct assessment of inWAX fermentation independent of BI in HFD-induced obese mice. It is therefore possible that inWAX alone exerts microbiota-dependent effects that partially contribute to the effects observed in the HFD + inWAX group. However, this does not weaken our central conclusion regarding the therapeutic potential of BI and inWAX as a synergistic synbiotic. Notably, BI mono-association experiments demonstrate that BI-mediated inWAX fermentation alone is sufficient to confer multiple beneficial effects, including expansion of health-promoting bile acids, increased systemic levels of anti-inflammatory and antioxidant phenolic compounds, reprogramming of lipid metabolism, and increased local and systemic immune protection against IBD.

MATERIALS AND METHODS

Bacteria culture

Bacteroides intestinalis DSM 17393 (BI) was cultured in an anaerobic workstation (Coy Laboratory Products) as previously described (PMID:18770533). Briefly, BI colonies were grown anaerobically at 37°C overnight in Brain Heart Infusion with Supplements (BHIS) medium. Bacterial growth was monitored by measuring the optical density at 600 nm (OD_{600}) using a spectrophotometer. For animal experiments, BI was cultured anaerobically until reaching log-phase growth (1.12×10^9 CFU mL^{-1}).

Mice

Ethics statement of animal use

All mice used in these experiments were housed at the University of Illinois Urbana Champaign (UIUC) and cared for according to the institutional 'Guide for the Care and Use of Laboratory Animals'. All procedures involving mouse care, euthanasia, and tissue collection were approved by the UIUC Animal Care and Use Committee (IACUC approved protocol #23096).

Diets

Custom chow diets for BI mono-associated mice were made by using the open standard diet (D11112201, Research Diets) as a base with the addition of 5%, 10%, or 15% inWAX. In the diets containing 5% or 10% inWAX, cellulose was proportionally added to make the total fiber 15%. In the diet containing 15% cellulose, 15% cellulose were added.

Custom high fat diet (HFD) diets for conventionally raised mice were made by using rodent *60% kcal% fat* diet (D12492, Research Diets) as a base, with inWAX or cellulose being added to reach 10%. The detailed diet compositions are provided in Supplementary Table 1. inWAX was purchased from Neogen Corporation, MI, USA (P-WAXYI, > 90% purity). Cellulose was provided by the Research Diets, Inc.

BI mono-association in standard chow diet-fed mice

Germ-free mice gastrically orally gavaged every other day with 200 μL of BHIS medium containing live BI (2.24×10^8 CFU/mL), heat-killed BI, or medium only (as vehicle control). The death of heat-killed BI was confirmed by incubating them anaerobically in BHIS broth at 37°C and their growth was monitored for up to 3 days. The viability of BI in live BI-inoculated mice was confirmed at various time points by assessing the colony-forming units (CFU) using fecal samples through conventional plating on BHIS agar. The Identity and specificity of BI in colonized mice were validated by sequencing PCR amplicons from their fecal microbial DNA using both universal 16S rRNA primers and BI strain-specific primers. Intestines were either flash-frozen or fixed in 4% paraformaldehyde for histomorphology or in Methacarn fixative for mucus architecture.

BI mono-association in inWAX or cellulose containing diet-treated mice

Germ-free mice were acclimated with inWAX or cellulose containing diets for 5 days, and then were gastrically gavaged BI every day. Body weight was monitored daily in all groups. Following euthanasia, tissues and serum were collected. The viability and specificity of BI in colonized mice

were validated by conventional plating and PCR-based sequencing as described above. Serum samples were processed for ferulic acid measurement or untargeted metabolomic profiling. Intestines were either flash-frozen or fixed in 4% paraformaldehyde for histological evaluation.

DSS-induced colitis

BI mono-associated mice received either 15% inWAX or 15% cellulose were treated with 2% (w/v) dextran sulfate sodium (DSS) in drinking water for 5 days (referred to as inWAX;DSS+ and cellu;DSS+, respectively). The control mice received 15% inWAX without DSS treatment (inWAX;DSS-). All mice were maintained on their respective diets throughout the DSS or water treatment period. Body weight and disease severity indicators, including soft feces, presence of blood in feces, and mild diarrhea, were monitored daily as clinical readouts of colitis. On day 5 of DSS treatment, mice were euthanized for tissue collection.

A range of physical parameters were evaluated, including gross colon morphology, colon length, spleen weight, spleen length, body weight.

For histological analyses, tissues were fixed in 4% paraformaldehyde and paraffin processed for histomorphology. Unless otherwise specified, tissue sections were cut at 5 µm thickness. Tissue sections were stained with hematoxylin and eosin (H&E) for morphology or Masson's Trichrome (MTC) for fibrosis. Goblet cells and mucus were visualized in Methacarn-fixed, paraffin-embedded sections using Alcian Blue (AB, pH 2.5). Images were acquired using a Keyence BZ-X810 microscope.

Histopathological scores were blindly assessed on each colon as described previously (PMID: 25197329). Briefly, each colon was assessed for four parameters: inflammatory cell infiltration, epithelial architecture destruction, crypt dilatation, and fibrosis within the mucosa, submucosa, and serosa. Significant histopathological features, such as loss of crypt structure, goblet cell depletion, mucosal erosion, and submucosal fibrosis were recorded to further distinguish the severity of colonic injury and inflammation.

Immunohistochemistry

For IHC on paraffin sections, sections were deparaffinized and subjected to heat-induced antigen retrieval using either sodium citrate buffer (10 mM sodium citrate, 0.05% Tween-20, pH 6.0) for 20 minutes. All sections were incubated overnight at 4°C with primary antibodies diluted in PBS containing 5% normal serum and 1% BSA. Detection was performed using Alexa 488 conjugated secondary antibody. Nuclei were counterstained with DAPI and imaged using a Nikon A1R confocal microscope.

Fluorescence in-situ hybridization (FISH)

BI-specific probe was designed according to established guidelines (PMID: 11692872). Following Alm et al. (1996) nomenclature, the probe was designated S-S-B.int-0461-a-S-22 and is referred to herein as "Bint461" for clarity and convenience. The probe was 5'-labeled with sulfonated fluorescein 488 (Sigma-Aldrich). To assess specificity, FISH was performed on pure cultures of BI and *Escherichia coli* as described by Zoetendal et al. (2002). Localization of BI in colon sections from mono-associated mice was assessed using the Bint461 probe. Total bacterial presence was simultaneously detected using a universal bacterial FISH probe, S-D-Bact-0338-a-

A-18 (Eub338), 5'-labeled with Texas Red as a positive control (Amann et al., 1990). The NONEUB338 probe, designed as the reverse complement of EUB338, was included as a negative control. Slides were counterstained with DAPI and images were acquired using a Nikon A1R confocal microscope.

Ferulic acid measurements

Absolute quantification of ferulic acid was done using Liquid Chromatography-tandem Mass Spectrometry (LC-MS/MS) by the Carver Metabolomics Core Facility at UIUC. Briefly, serum samples were spiked with a mixture of deuterium- and stable isotope-labeled internal standards prior to alkaline hydrolysis with NaOH, which facilitated the release of ferulic acid from its conjugated forms. Total ferulic acid content, comprising both free ferulic acid and that liberated from conjugates, was subsequently quantified.

Untargeted metabolomics

Sample preparation

Samples were spiked with isotope-labeled internal standards prior to extraction and processed for untargeted metabolomics by the Carver Metabolomics Core at the Roy J. Carver Biotechnology Center (University of Illinois Urbana-Champaign). A 1 µL aliquot of each processed sample was injected for analysis. Plasma and fecal samples were analyzed in separate batches, and fecal samples were normalized to input dry weight.

LC–MS analysis

Metabolomic profiling was performed using a Dionex Ultimate 3000 UHPLC system coupled to a Q-Exactive mass spectrometer (Thermo Scientific). Metabolites were separated by reversed-phase chromatography on a Waters Acquity BEH C18 column (100 × 2.1 mm, 1.7 µm) maintained at 30 °C with a flow rate of 0.3 mL/min, using a water/acetonitrile gradient containing 0.1% formic acid. Data were acquired in both positive and negative electrospray ionization modes.

Data processing and analysis

Raw LC–MS data were processed using MS-DIAL (v4.90) for feature detection, alignment, adduct annotation, and compound identification based on accurate mass, MS/MS spectra, and retention time matching to an in-house standards library and public databases (MoNA, MassBank, GNPS, METLIN, and NIST20). Features with a sample-to-blank ratio <10 were excluded, and metabolites were assigned confidence levels according to Metabolomics Standards Initiative (MSI) guidelines. Positive and negative ionization datasets were merged, duplicate features were removed using quality control metrics, and peak intensities were normalized to internal standards. Principal component analysis was used for data quality assessment and outlier detection.

Metabolomics Data Processing and Statistical Analysis

Pairwise comparisons between experimental groups were performed using a custom function that calculated log2 fold changes and p-values for each metabolite. Zero values were excluded prior to analysis. Log2-transformed metabolite intensities were compared between groups using t-tests assuming unequal variance. P-values were adjusted for multiple testing using the false discovery rate (FDR) method. Significant metabolites were defined based on both p-value (<0.05) and log2 fold change thresholds. Volcano plots were generated to highlight significant up- and down-

regulated metabolites. Heatmaps of selected metabolites were created with row-standardization (Z-score) applied.

To investigate shared and unique metabolites across group comparisons, Venn diagrams and UpSet plots were constructed. Metabolites were classified as "unique" or "shared" based on their occurrence across comparisons, and compound class information was retrieved from external databases. Pie charts were generated to visualize the distribution of metabolite categories for up- and down-regulated metabolites across group comparisons.

All data processing, statistical analyses, and visualizations were performed in R (v4.5.1) using the following packages: ggplot2 (v4.0.1) [72], ggrepel (v0.9.6)[73]], ComplexHeatmap (v2.16.0)[74], patchwork (v1.3.2)[75], dplyr (v1.1.4), tidyr (v1.3.1), tibble (v3.3.0),and readxl (v1.4.5) [72].

RNA-sequencing analysis

RNAs were extracted from the colons and spleens using PureLink RNA Mini Kit (Ambion, Cat. 12183025). RNA-seq libraries were constructed and sequenced at the UIUC Biotechnology Center High-Throughput Sequencing Core. Each library generated over 80 million single-end reads.

Adaptor sequences and low-quality bases were removed from the raw sequencing data using Trimmomatic v0.39. [76] Transcript abundance was quantified using Kallisto v0.44.0 [77], aligning reads to the mouse transcriptome (GRCm39, Ensembl). Data quality and sample consistency were evaluated through principal component analysis (PCA) and hierarchical clustering based on transcript quantifications. Transcript-level expression values corresponding to the same gene were then aggregated to obtain gene-level expression estimates. Differentially expressed genes (DEGs) were identified using DESeq2 v2_1.46.0 [78], with a significance threshold of adjusted p-value < 0.05 and $|\log2 \text{ fold change}| > 1$. Gene Ontology (GO) functional enrichment analysis was performed using Metascape (https://metascape.org/) [79] to identify significantly enriched biological processes, molecular functions, and cellular components.

Immune Cell Fraction Analysis

Immune cell composition was estimated from bulk RNA-seq data using a deconvolution-based approach implemented in the R package immunedeconv (https://github.com/omnideconv/immunedeconv) [80]. Mouse gene symbols were converted to their human orthologs using the convert_human_mouse_genes function. Immune cell fractions were inferred using quanTIseq [81], a constrained least squares regression method, with all expressed genes (TPM as the unit) to deconvolute the relative proportions of immune cell populations within each sample.

Quantitative Real-Time PCR

RNAs were extracted using TRIzol reagent according to standard protocols. Real-time PCR reactions were performed blindly in duplicate using SYBR green master mix.

Statistical analysis

Graphs were generated using R or GraphPad Prism software. Data normality was assessed using the Shapiro–Wilk test. Statistical significance between experimental and control groups was

determined using a two-tailed unpaired Student's *t*-test or a two-tailed Mann-Whitney U test, unless otherwise specified.

ACKNOWLEDGMENTS

We thank Dr. Bo Wang, Ms. Tiantian Yang, and Mr. Zhiming Zhao (Department of Biosciences) for technical assistance with metabolic parameter measurements. We thank Dr. Alexander Ulanov, Dr. Michael Frano, and Ms. Wei Lu at the Metabolomics Core of the Roy J. Carver Biotechnology Center, University of Illinois Urbana-Champaign, for assistance with metabolomics data processing. We thank Karen Doty (Histology Laboratory) for assistance with histological staining.

FUNDING

This work was supported by the National Institutes of Health (GM140306 to W.M. and I.C.; ES036194 to W.M. and J.Y.; and GM131810 to J.Y.), the University of Illinois Urbana-Champaign Campus Research Board funds (to W.M.), and the UIUC Gnotobiotic Facility seed funds (to W.M.).

CONFLICT OF INTEREST: The authors declare no conflict of interest.

References

1. Makki, K., Deehan, E.C., Walter, J., and Backhed, F. (2018). The Impact of Dietary Fiber on Gut Microbiota in Host Health and Disease. Cell Host Microbe *23*, 705-715. 10.1016/j.chom.2018.05.012.
2. Khan, N.A., Raine, L.B., Drollette, E.S., Scudder, M.R., Kramer, A.F., and Hillman, C.H. (2015). Dietary fiber is positively associated with cognitive control among prepubertal children. J Nutr *145*, 143-149. 10.3945/jn.114.198457.
3. Prokopidis, K., Giannos, P., Ispoglou, T., Witard, O.C., and Isanejad, M. (2022). Dietary Fiber Intake is Associated with Cognitive Function in Older Adults: Data from the National Health and Nutrition Examination Survey. Am J Med *135*, e257-e262. 10.1016/j.amjmed.2022.03.022.
4. Zhang, D., Sheng, J., Chen, L., Cheng, D., Cao, Y., Su, Y., Jiang, Y., Liu, W., Yu, Y., Jia, H., et al. (2023). Effects of Dietary Fiber on the Risk of Gestational Diabetes Mellitus in Advanced Maternal Age Women: Study Protocol for a Randomized Controlled Trial. Mol Nutr Food Res *67*, e2200437. 10.1002/mnfr.202200437.
5. Liu, X.F., Shao, J.H., Liao, Y.T., Wang, L.N., Jia, Y., Dong, P.J., Liu, Z.Z., He, D.D., Li, C., and Zhang, X. (2023). Regulation of short-chain fatty acids in the immune system. Front Immunol *14*, 1186892. 10.3389/fimmu.2023.1186892.
6. Liu, P., Wang, Y., Yang, G., Zhang, Q., Meng, L., Xin, Y., and Jiang, X. (2021). The role of short-chain fatty acids in intestinal barrier function, inflammation, oxidative stress, and colonic carcinogenesis. Pharmacol Res *165*, 105420. 10.1016/j.phrs.2021.105420.
7. Munte, E., and Hartmann, P. (2025). The Role of Short-Chain Fatty Acids in Metabolic Dysfunction-Associated Steatotic Liver Disease and Other Metabolic Diseases. Biomolecules *15*. 10.3390/biom15040469.
8. Silva, Y.P., Bernardi, A., and Frozza, R.L. (2020). The Role of Short-Chain Fatty Acids From Gut Microbiota in Gut-Brain Communication. Front Endocrinol (Lausanne) *11*, 25. 10.3389/fendo.2020.00025.
9. Grant, E.T., De Franco, H., and Desai, M.S. (2025). Non-SCFA microbial metabolites associated with fiber fermentation and host health. Trends Endocrinol Metab *36*, 70-82. 10.1016/j.tem.2024.06.009.
10. Pereira, G.V., Abdel-Hamid, A.M., Dutta, S., D'Alessandro-Gabazza, C.N., Wefers, D., Farris, J.A., Bajaj, S., Wawrzak, Z., Atomi, H., Mackie, R.I., et al. (2021). Degradation of complex arabinoxylans by human colonic Bacteroidetes. Nat Commun *12*, 459. 10.1038/s41467-020-20737-5.
11. P, N.P.V., and Joye, I.J. (2020). Dietary Fibre from Whole Grains and Their Benefits on Metabolic Health. Nutrients *12*. 10.3390/nu12103045.
12. Chen, Z., Mense, A.L., Brewer, L.R., and Shi, Y.C. (2024). Wheat bran arabinoxylans: Chemical structure, extraction, properties, health benefits, and uses in foods. Compr Rev Food Sci Food Saf *23*, e13366. 10.1111/1541-4337.13366.
13. Ozcan, U., Yilmaz, E., Ozcan, L., Furuhashi, M., Vaillancourt, E., Smith, R.O., Gorgun, C.Z., and Hotamisligil, G.S. (2006). Chemical chaperones reduce ER stress and restore glucose homeostasis in a mouse model of type 2 diabetes. Science *313*, 1137-1140. 10.1126/science.1128294.
14. Kars, M., Yang, L., Gregor, M.F., Mohammed, B.S., Pietka, T.A., Finck, B.N., Patterson, B.W., Horton, J.D., Mittendorfer, B., Hotamisligil, G.S., and Klein, S. (2010).

Tauroursodeoxycholic Acid may improve liver and muscle but not adipose tissue insulin sensitivity in obese men and women. Diabetes *59*, 1899-1905. 10.2337/db10-0308.
15. Zheng, X., Chen, T., Jiang, R., Zhao, A., Wu, Q., Kuang, J., Sun, D., Ren, Z., Li, M., Zhao, M., et al. (2021). Hyocholic acid species improve glucose homeostasis through a distinct TGR5 and FXR signaling mechanism. Cell Metab *33*, 791-803 e797. 10.1016/j.cmet.2020.11.017.
16. Zheng, X., Chen, T., Zhao, A., Ning, Z., Kuang, J., Wang, S., You, Y., Bao, Y., Ma, X., Yu, H., et al. (2021). Hyocholic acid species as novel biomarkers for metabolic disorders. Nat Commun *12*, 1487. 10.1038/s41467-021-21744-w.
17. Cefalu, A.B., Spina, R., Noto, D., Valenti, V., Ingrassia, V., Giammanco, A., Panno, M.D., Ganci, A., Barbagallo, C.M., and Averna, M.R. (2015). Novel CREB3L3 Nonsense Mutation in a Family With Dominant Hypertriglyceridemia. Arterioscler Thromb Vasc Biol *35*, 2694-2699. 10.1161/ATVBAHA.115.306170.
18. Dron, J.S., Dilliott, A.A., Lawson, A., McIntyre, A.D., Davis, B.D., Wang, J., Cao, H., Movsesyan, I., Malloy, M.J., Pullinger, C.R., et al. (2020). Loss-of-Function CREB3L3 Variants in Patients With Severe Hypertriglyceridemia. Arterioscler Thromb Vasc Biol *40*, 1935-1941. 10.1161/ATVBAHA.120.314168.
19. Gurevitz, C., Mechanick, J.I., Do, R., and Rosenson, R.S. (2025). Hypertriglyceridemia-induced acute pancreatitis in pregnancy associated with CREB3L3 mutation. J Clin Lipidol *19*, 173-177. 10.1016/j.jacl.2024.10.001.
20. Nakagawa, Y., Satoh, A., Tezuka, H., Han, S.I., Takei, K., Iwasaki, H., Yatoh, S., Yahagi, N., Suzuki, H., Iwasaki, Y., et al. (2016). CREB3L3 controls fatty acid oxidation and ketogenesis in synergy with PPARalpha. Sci Rep *6*, 39182. 10.1038/srep39182.
21. Siepka, S.M., Yoo, S.H., Park, J., Song, W., Kumar, V., Hu, Y., Lee, C., and Takahashi, J.S. (2007). Circadian mutant Overtime reveals F-box protein FBXL3 regulation of cryptochrome and period gene expression. Cell *129*, 1011-1023. 10.1016/j.cell.2007.04.030.
22. Goriki, A., Hatanaka, F., Myung, J., Kim, J.K., Yoritaka, T., Tanoue, S., Abe, T., Kiyonari, H., Fujimoto, K., Kato, Y., et al. (2014). A novel protein, CHRONO, functions as a core component of the mammalian circadian clock. PLoS Biol *12*, e1001839. 10.1371/journal.pbio.1001839.
23. Gachon, F. (2007). Physiological function of PARbZip circadian clock-controlled transcription factors. Ann Med *39*, 562-571. 10.1080/07853890701491034.
24. Campbell, N.K., Fitzgerald, H.K., and Dunne, A. (2021). Regulation of inflammation by the antioxidant haem oxygenase 1. Nat Rev Immunol *21*, 411-425. 10.1038/s41577-020-00491-x.
25. Zannas, A.S., Wiechmann, T., Gassen, N.C., and Binder, E.B. (2016). Gene-Stress-Epigenetic Regulation of FKBP5: Clinical and Translational Implications. Neuropsychopharmacology *41*, 261-274. 10.1038/npp.2015.235.
26. Ravenna, L., Salvatori, L., and Russo, M.A. (2016). HIF3alpha: the little we know. FEBS J *283*, 993-1003. 10.1111/febs.13572.
27. Barone, S., Fussell, S.L., Singh, A.K., Lucas, F., Xu, J., Kim, C., Wu, X., Yu, Y., Amlal, H., Seidler, U., et al. (2009). Slc2a5 (Glut5) is essential for the absorption of fructose in the intestine and generation of fructose-induced hypertension. J Biol Chem *284*, 5056-5066. 10.1074/jbc.M808128200.

28. Horsey, A.J., Cox, M.H., Sarwat, S., and Kerr, I.D. (2016). The multidrug transporter ABCG2: still more questions than answers. Biochem Soc Trans *44*, 824-830. 10.1042/BST20160014.
29. Istiaq, A., and Ohta, K. (2022). A review on Tsukushi: mammalian development, disorders, and therapy. J Cell Commun Signal *16*, 505-513. 10.1007/s12079-022-00669-z.
30. Tabibzadeh, S., and Hemmati-Brivanlou, A. (2006). Lefty at the crossroads of "stemness" and differentiative events. Stem Cells *24*, 1998-2006. 10.1634/stemcells.2006-0075.
31. Shindo, R., Katagiri, T., Komazawa-Sakon, S., Ohmuraya, M., Takeda, W., Nakagawa, Y., Nakagata, N., Sakuma, T., Yamamoto, T., Nishiyama, C., et al. (2020). Regenerating islet-derived protein (Reg)3beta plays a crucial role in attenuation of ileitis and colitis in mice. Biochem Biophys Rep *21*, 100738. 10.1016/j.bbrep.2020.100738.
32. van Ampting, M.T., Loonen, L.M., Schonewille, A.J., Konings, I., Vink, C., Iovanna, J., Chamaillard, M., Dekker, J., van der Meer, R., Wells, J.M., and Bovee-Oudenhoven, I.M. (2012). Intestinally secreted C-type lectin Reg3b attenuates salmonellosis but not listeriosis in mice. Infect Immun *80*, 1115-1120. 10.1128/IAI.06165-11.
33. Wang, L., Fouts, D.E., Starkel, P., Hartmann, P., Chen, P., Llorente, C., DePew, J., Moncera, K., Ho, S.B., Brenner, D.A., et al. (2016). Intestinal REG3 Lectins Protect against Alcoholic Steatohepatitis by Reducing Mucosa-Associated Microbiota and Preventing Bacterial Translocation. Cell Host Microbe *19*, 227-239. 10.1016/j.chom.2016.01.003.
34. Shrestha, N., Bahnan, W., Wiley, D.J., Barber, G., Fields, K.A., and Schesser, K. (2012). Eukaryotic initiation factor 2 (eIF2) signaling regulates proinflammatory cytokine expression and bacterial invasion. J Biol Chem *287*, 28738-28744. 10.1074/jbc.M112.375915.
35. Ku, Y.C., Lai, M.H., Lo, C.C., Cheng, Y.C., Qiu, J.T., Tarn, W.Y., and Lai, M.C. (2019). DDX3 Participates in Translational Control of Inflammation Induced by Infections and Injuries. Mol Cell Biol *39*. 10.1128/MCB.00285-18.
36. Cunningham, C.M., Li, M., Ruffenach, G., Doshi, M., Aryan, L., Hong, J., Park, J., Hrncir, H., Medzikovic, L., Umar, S., et al. (2022). Y-Chromosome Gene, Uty, Protects Against Pulmonary Hypertension by Reducing Proinflammatory Chemokines. Am J Respir Crit Care Med *206*, 186-196. 10.1164/rccm.202110-2309OC.
37. Chen, J., Wang, T., Zhang, D., Wang, H., Huang, Z., Yang, Z., Li, J., Hu, T., Wang, X., and Li, X. (2024). KDM5D histone demethylase mediates p38alpha inactivation via its enzymatic activity to inhibit cancer progression. Proc Natl Acad Sci U S A *121*, e2402022121. 10.1073/pnas.2402022121.
38. Liu, X., and Secombe, J. (2015). The Histone Demethylase KDM5 Activates Gene Expression by Recognizing Chromatin Context through Its PHD Reader Motif. Cell Rep *13*, 2219-2231. 10.1016/j.celrep.2015.11.007.
39. Kawano, N., Araki, N., Yoshida, K., Hibino, T., Ohnami, N., Makino, M., Kanai, S., Hasuwa, H., Yoshida, M., Miyado, K., and Umezawa, A. (2014). Seminal vesicle protein SVS2 is required for sperm survival in the uterus. Proc Natl Acad Sci U S A *111*, 4145-4150. 10.1073/pnas.1320715111.
40. Flowers, M.T., and Ntambi, J.M. (2008). Role of stearoyl-coenzyme A desaturase in regulating lipid metabolism. Curr Opin Lipidol *19*, 248-256. 10.1097/MOL.0b013e3282f9b54d.

41. Chen, C., Shah, Y.M., Morimura, K., Krausz, K.W., Miyazaki, M., Richardson, T.A., Morgan, E.T., Ntambi, J.M., Idle, J.R., and Gonzalez, F.J. (2008). Metabolomics reveals that hepatic stearoyl-CoA desaturase 1 downregulation exacerbates inflammation and acute colitis. Cell Metab *7*, 135-147. 10.1016/j.cmet.2007.12.003.
42. Pallotta, M.T., Rossini, S., Suvieri, C., Coletti, A., Orabona, C., Macchiarulo, A., Volpi, C., and Grohmann, U. (2022). Indoleamine 2,3-dioxygenase 1 (IDO1): an up-to-date overview of an eclectic immunoregulatory enzyme. FEBS J *289*, 6099-6118. 10.1111/febs.16086.
43. Kenney, L.L., Chiu, R.S., Dutra, M.N., Wactor, A., Honan, C., Shelerud, L., Corrigan, J.J., Yu, K., Ferrari, J.D., Jeffrey, K.L., et al. (2024). mRNA-delivery of IDO1 suppresses T cell-mediated autoimmunity. Cell Rep Med *5*, 101717. 10.1016/j.xcrm.2024.101717.
44. Gao, Z., Shao, S., Xu, Z., Nie, J., Li, C., and Du, C. (2025). IDO1 induced macrophage M1 polarization via ER stress-associated GRP78-XBP1 pathway to promote ulcerative colitis progression. Front Med (Lausanne) *12*, 1524952. 10.3389/fmed.2025.1524952.
45. Pejler, G., Ronnberg, E., Waern, I., and Wernersson, S. (2010). Mast cell proteases: multifaceted regulators of inflammatory disease. Blood *115*, 4981-4990. 10.1182/blood-2010-01-257287.
46. Marti, I.L.A.A., and Reith, W. (2021). Arginine-dependent immune responses. Cell Mol Life Sci *78*, 5303-5324. 10.1007/s00018-021-03828-4.
47. Asosingh, K., Lauruschkat, C.D., Alemagno, M., Frimel, M., Wanner, N., Weiss, K., Kessler, S., Meyers, D.A., Bennett, C., Xu, W., and Erzurum, S. (2020). Arginine metabolic control of airway inflammation. JCI Insight *5*. 10.1172/jci.insight.127801.
48. De Santi, C., Nally, F.K., Afzal, R., Duffy, C.P., Fitzsimons, S., Annett, S.L., Robson, T., Dowling, J.K., Cryan, S.A., and McCoy, C.E. (2022). Enhancing arginase 2 expression using target site blockers as a strategy to modulate macrophage phenotype. Mol Ther Nucleic Acids *29*, 643-655. 10.1016/j.omtn.2022.08.004.
49. Dowling, J.K., Afzal, R., Gearing, L.J., Cervantes-Silva, M.P., Annett, S., Davis, G.M., De Santi, C., Assmann, N., Dettmer, K., Gough, D.J., et al. (2021). Mitochondrial arginase-2 is essential for IL-10 metabolic reprogramming of inflammatory macrophages. Nat Commun *12*, 1460. 10.1038/s41467-021-21617-2.
50. Millet, V., Gensollen, T., Maltese, M., Serrero, M., Lesavre, N., Bourges, C., Pitaval, C., Cadra, S., Chasson, L., Vu Man, T.P., et al. (2023). Harnessing the Vnn1 pantetheinase pathway boosts short chain fatty acids production and mucosal protection in colitis. Gut *72*, 1115-1128. 10.1136/gutjnl-2021-325792.
51. Kersten, S. (2021). Role and mechanism of the action of angiopoietin-like protein ANGPTL4 in plasma lipid metabolism. J Lipid Res *62*, 100150. 10.1016/j.jlr.2021.100150.
52. Li, J., and Dawson, P.A. (2019). Animal models to study bile acid metabolism. Biochim Biophys Acta Mol Basis Dis *1865*, 895-911. 10.1016/j.bbadis.2018.05.011.
53. Eyssen, H.J., De Pauw, G., and Van Eldere, J. (1999). Formation of hyodeoxycholic acid from muricholic acid and hyocholic acid by an unidentified gram-positive rod termed HDCA-1 isolated from rat intestinal microflora. Appl Environ Microbiol *65*, 3158-3163. 10.1128/AEM.65.7.3158-3163.1999.
54. Sehayek, E., Ono, J.G., Duncan, E.M., Batta, A.K., Salen, G., Shefer, S., Neguyen, L.B., Yang, K., Lipkin, M., and Breslow, J.L. (2001). Hyodeoxycholic acid efficiently

suppresses atherosclerosis formation and plasma cholesterol levels in mice. J Lipid Res *42*, 1250-1256.
55. Zhong, J., He, X., Gao, X., Liu, Q., Zhao, Y., Hong, Y., Zhu, W., Yan, J., Li, Y., Li, Y., et al. (2023). Hyodeoxycholic acid ameliorates nonalcoholic fatty liver disease by inhibiting RAN-mediated PPARalpha nucleus-cytoplasm shuttling. Nat Commun *14*, 5451. 10.1038/s41467-023-41061-8.
56. Kuang, J., Wang, J., Li, Y., Li, M., Zhao, M., Ge, K., Zheng, D., Cheung, K.C.P., Liao, B., Wang, S., et al. (2023). Hyodeoxycholic acid alleviates non-alcoholic fatty liver disease through modulating the gut-liver axis. Cell Metab *35*, 1752-1766 e1758. 10.1016/j.cmet.2023.07.011.
57. Oluwole, O., Fernando, W.B., Lumanlan, J., Ademuyiwa, O., and Jayasena, V. (2022). Role of phenolic acid, tannins, stilbenes, lignans and flavonoids in human health – a review. International Journal of Food Science and Technology *57*, 6326-6335. 10.1111/ijfs.15936.
58. Zhang, Y., Cai, P., Cheng, G., and Zhang, Y. (2022). A Brief Review of Phenolic Compounds Identified from Plants: Their Extraction, Analysis, and Biological Activity. Natural Product Communications *17*, 1934578X211069721. 10.1177/1934578x211069721.
59. Landete, J.M. (2012). Plant and mammalian lignans: A review of source, intake, metabolism, intestinal bacteria and health. Food Research International *46*, 410-424. https://doi.org/10.1016/j.foodres.2011.12.023.
60. Heinonen, S., Nurmi, T., Liukkonen, K., Poutanen, K., Wahala, K., Deyama, T., Nishibe, S., and Adlercreutz, H. (2001). In vitro metabolism of plant lignans: new precursors of mammalian lignans enterolactone and enterodiol. J Agric Food Chem *49*, 3178-3186. 10.1021/jf010038a.
61. Amaral, J.D., Viana, R.J., Ramalho, R.M., Steer, C.J., and Rodrigues, C.M. (2009). Bile acids: regulation of apoptosis by ursodeoxycholic acid. J Lipid Res *50*, 1721-1734. 10.1194/jlr.R900011-JLR200.
62. Engin, F., Yermalovich, A., Nguyen, T., Hummasti, S., Fu, W., Eizirik, D.L., Mathis, D., and Hotamisligil, G.S. (2013). Restoration of the unfolded protein response in pancreatic beta cells protects mice against type 1 diabetes. Sci Transl Med *5*, 211ra156. 10.1126/scitranslmed.3006534.
63. Bronczek, G.A., Vettorazzi, J.F., Soares, G.M., Kurauti, M.A., Santos, C., Bonfim, M.F., Carneiro, E.M., Balbo, S.L., Boschero, A.C., and Costa Junior, J.M. (2019). The Bile Acid TUDCA Improves Beta-Cell Mass and Reduces Insulin Degradation in Mice With Early-Stage of Type-1 Diabetes. Front Physiol *10*, 561. 10.3389/fphys.2019.00561.
64. Ochiai, T., Nagayama, T., Matsui, K., Amano, K., Sano, T., Wakabayashi, T., and Iwatsubo, T. (2021). Tauroursodeoxycholic Acid Attenuates Diet-Induced and Age-Related Peripheral Endoplasmic Reticulum Stress and Cerebral Amyloid Pathology in a Mouse Model of Alzheimer's Disease. J Prev Alzheimers Dis *8*, 483-494. 10.14283/jpad.2021.33.
65. Kusaczuk, M. (2019). Tauroursodeoxycholate-Bile Acid with Chaperoning Activity: Molecular and Cellular Effects and Therapeutic Perspectives. Cells *8*. 10.3390/cells8121471.
66. Si, Z.L., Wang, H.Y., Wang, T., Cao, Y.Z., Li, Q.Z., Liu, K., Huang, Z., Liu, H.L., Tan, Y.J., Wang, Y.Y., et al. (2024). Gut Bacteroides ovatus ameliorates renal fibrosis by

promoting the production of HDCA through upregulation of Clostridium scindens. Cell Rep *43*, 114830. 10.1016/j.celrep.2024.114830.
67. Kyoko, O.O., Kono, H., Ishimaru, K., Miyake, K., Kubota, T., Ogawa, H., Okumura, K., Shibata, S., and Nakao, A. (2014). Expressions of tight junction proteins Occludin and Claudin-1 are under the circadian control in the mouse large intestine: implications in intestinal permeability and susceptibility to colitis. PLoS One *9*, e98016. 10.1371/journal.pone.0098016.
68. Nagao, Y., Taguchi, A., and Ohta, Y. (2025). Circadian Rhythm Dysregulation in Inflammatory Bowel Disease: Mechanisms and Chronotherapeutic Approaches. Int J Mol Sci *26*. 10.3390/ijms26083724.
69. Liu, X., Yu, R., Zhu, L., Hou, X., and Zou, K. (2017). Bidirectional Regulation of Circadian Disturbance and Inflammation in Inflammatory Bowel Disease. Inflamm Bowel Dis *23*, 1741-1751. 10.1097/MIB.0000000000001265.
70. Ye, Y., Liu, C., Wu, R., Kang, D., Gao, H., Lv, H., Feng, Z., Shi, Y., Liu, Z., and Chen, L. (2024). Circadian clock component PER2 negatively regulates CD4(+) T cell IFN-gamma production in ulcerative colitis. Mucosal Immunol *17*, 1161-1173. 10.1016/j.mucimm.2024.07.010.
71. Pagel, R., Bar, F., Schroder, T., Sunderhauf, A., Kunstner, A., Ibrahim, S.M., Autenrieth, S.E., Kalies, K., Konig, P., Tsang, A.H., et al. (2017). Circadian rhythm disruption impairs tissue homeostasis and exacerbates chronic inflammation in the intestine. FASEB J *31*, 4707-4719. 10.1096/fj.201700141RR.
72. Wickham, H. (2016). ggplot2 Elegant Graphics for Data Analysis (Springer).
73. K, S. (2018). ggrepel: Automatically Position Non-Overlapping Text Labels with 'ggplot2'. R package version 0.9.6.9999.
74. Gu, Z., Eils, R., and Schlesner, M. (2016). Complex heatmaps reveal patterns and correlations in multidimensional genomic data. Bioinformatics *32*, 2847-2849. 10.1093/bioinformatics/btw313.
75. T, P. (2019). patchwork: The Composer of Plots. R package version 1.3.
76. Bolger, A.M., Lohse, M., and Usadel, B. (2014). Trimmomatic: a flexible trimmer for Illumina sequence data. Bioinformatics *30*, 2114-2120. 10.1093/bioinformatics/btu170.
77. Bray, N.L., Pimentel, H., Melsted, P., and Pachter, L. (2016). Near-optimal probabilistic RNA-seq quantification. Nat Biotechnol *34*, 525-527. 10.1038/nbt.3519.
78. Love, M.I., Huber, W., and Anders, S. (2014). Moderated estimation of fold change and dispersion for RNA-seq data with DESeq2. Genome Biol *15*, 550. 10.1186/s13059-014-0550-8.
79. Zhou, Y., Zhou, B., Pache, L., Chang, M., Khodabakhshi, A.H., Tanaseichuk, O., Benner, C., and Chanda, S.K. (2019). Metascape provides a biologist-oriented resource for the analysis of systems-level datasets. Nat Commun *10*, 1523. 10.1038/s41467-019-09234-6.
80. Sturm, G., Finotello, F., and List, M. (2020). Immunedeconv: An R Package for Unified Access to Computational Methods for Estimating Immune Cell Fractions from Bulk RNA-Sequencing Data. Methods Mol Biol *2120*, 223-232. 10.1007/978-1-0716-0327-7_16.
81. Finotello, F., Mayer, C., Plattner, C., Laschober, G., Rieder, D., Hackl, H., Krogsdam, A., Loncova, Z., Posch, W., Wilflingseder, D., et al. (2019). Molecular and pharmacological modulators of the tumor immune contexture revealed by deconvolution of RNA-seq data. Genome Med *11*, 34. 10.1186/s13073-019-0638-6.

Figure legends

Figure 1. BI mono-association reduces mouse cecum size and enhances intestinal mucus secretion

(A) Schematic of the experimental design and treatments for each mouse group. (B) Representative images of the small intestine, cecum, and colon from mice in each group, with the ratio of cecum size and weight to body weight quantification shown on the right. (C) Alcian blue staining shows increased number of goblet cells in the colon of BI-inoculated mice. Quantification is shown on right. (D) Alcian blue-BHG staining showing increased thickness of colon mucus layer in BI-inoculated mice. Scale bars, 50 µm. * $p < 0.05$; **** $p < 0.0001$.

Figure 2. **BI and inWAX increased beneficial bile acids and phenolic compounds.**

(A) Schematic of the experimental workflow and treatments for each mouse group. (B) Comparison of systemic levels of ferulic acid across 6 groups of mice. (C) Principal Component Analysis (PCA) showing distinct circulating metabolite profiles induced by inWAX versus cellulose in BI mono-associated mice. (D) Volcano plot showing differentially abundant circulating metabolites in inWAX-fed mice relative to cellulose-fed mice; bile acids are highlighted in green and phenolic compounds in purple. (E) Heatmaps showing inWAX-induced increases in phenolic compounds and bile acids. (F) Comparison of the GSH/GSSG ratio. * $p < 0.05$, 1-tailed T test. (G) Heatmaps showing inWAX-induced reductions in lysophosphatidylcholines (LPCs) and carnitine derivatives.

Figure 3. BI and inWAX activates genes essential for circadian regulation and triglyceride metabolism in the colon

(A) The volcano plot showing differentially expressed gene in the colon of inWAX-fed mice relative to the cellulose-fed mice. Circadian regulators are highlighted in blue and *Creb3l3* in red. (B) Schematic illustrating the roles of upregulated circadian regulatory genes within the circadian clock network. (C) Quantitative RT-PCR validation of selected upregulated genes. Expression levels were normalized to *Gapdh*. Each symbol represents an individual mouse; bars indicate mean values. * $p < 0.05$.

Figure 4. BI and inWAX ameliorates DSS-induced colitis

(A) Experimental schematic showing dietary acclimation, BI inoculation, and DSS treatment. Germ-free mice were acclimated to customized diets for 5 days, inoculated with BI, and treated with or without DSS for an additional 5 days. Compared with the cellu;DSS+ group, mice in the inWAX;DSS+ group exhibited reduced body weight loss (B), decreased splenomegaly (C), and lower histopathological scores for inflammation, crypt dilation, and fibrosis (D). Masson's Trichrome staining (blue in D) marks fibrosis. Bars represent 50 µm.

Figure 5. BI and inWAX remodels the colonic transcriptome in response to DSS.

(A) Volcano plot showing differentially expressed genes in the colons of inWAX-fed mice relative to cellulose-fed mice following DSS treatment. Y chromosome-linked genes are circled in blue and *Reg3b* is circled in red. (B) Gene Ontology (GO) analysis showing enrichment of lipid metabolism pathways among upregulated genes. (C) Heatmap showing upregulated metabolic genes. (D) GO analysis showing enrichment of wound-healing pathways among downregulated genes.

Figure 6. BI and inWAX reshape the spleen immune cell landscape in response to DSS.
(A) H&E-stained spleen sections showing enlarged white pulp regions in inWAX-treated mice (arrows). (B) GO analysis showing enrichment of lymphocyte expansion and adaptive immune response pathways among genes upregulated by BI-inWAX. (C) GO analysis showing enrichment of cell division pathways among downregulated genes. (D) Stacked bar plot showing relative proportions of splenic immune cell lineages. (E) Bar plots showing statistically significant differences in immune cell proportions between inWAX- and cellulose-treated mice. (F) Heatmap showing genes upregulated in both the colon and spleen, including Y-linked and metabolic genes.

Figure 7. BI and inWAX improves glucose tolerance and bile acid profiles in HFD-induced obesity
(A) Schematic of the experimental workflow illustrating BI- and inWAX-based interventions in HFD-induced obese mice. All mice were inoculated with BI. (B) PCR validation of fecal BI abundance at indicated time points. Note BI is not a native resident of B6 mice. (C) Glucose tolerance test results showing improved glucose clearance in inWAX-treated mice relative to HFD controls. (D) BI and inWAX enhance the production of beneficial bile acids, HCA and HDCA, but not their precursors. * $p < 0.05$. ns, not significant.

Figure 8. BI and inWAX rewire gut metabolic outputs under HFD conditions
(A) Principal component analysis showing BI-inWAX induced a metabolite profile distinct from cellulose. (B) The UpSet plot showing metabolites uniquely or commonly altered among the indicated groups. (C) Pie chart showing structural classification of metabolites uniquely induced by BI-inWAX. (D) Heatmap showing increased production of neurotransmitters and their precursors. (E) Heatmap showing BI-inWAX-induced increases in microbial fermentation-derived bioactive phenolic compounds and vitamins, alongside reduced levels of plant-derived polyphenols. (F) Heatmap showing BI-inWAX downregulated **phosphatidylcholine** derivatives.

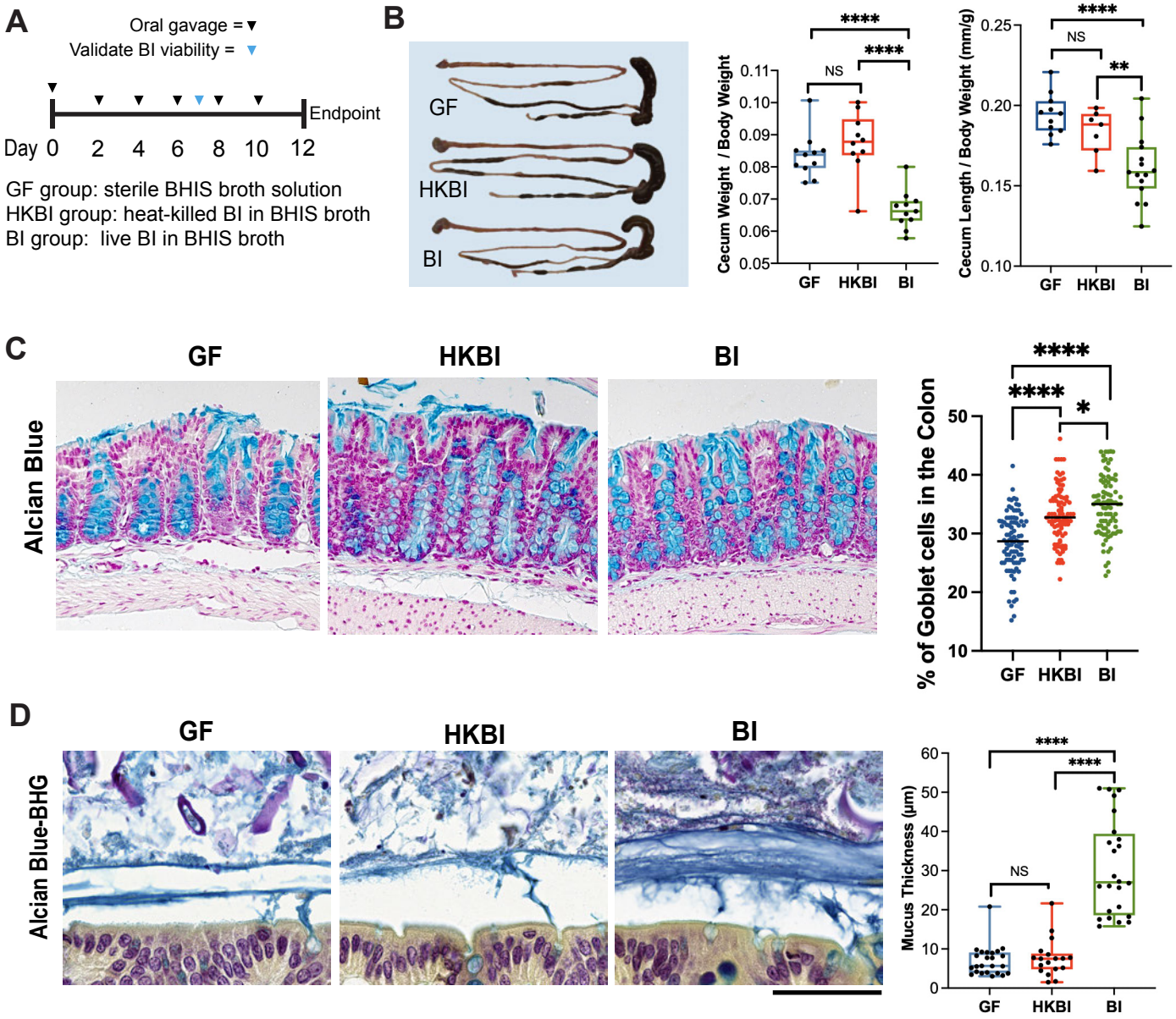
A
Oral gavage =
Validate BI viability =
Endpoint
Day 0 2 4 6 8 10 12
GF group: sterile BHIS broth solution
HKBI group: heat-killed BI in BHIS broth
BI group: live BI in BHIS broth
B
GF
HKBI
BI
Cecum Weight / Body Weight
Cecum Length / Body Weight (mm/g)
NS
****
**
C
GF
HKBI
BI
Alcian Blue
% of Goblet cells in the Colon
*
D
Alcian Blue-BHG
Mucus Thickness (µm)

Figure 1

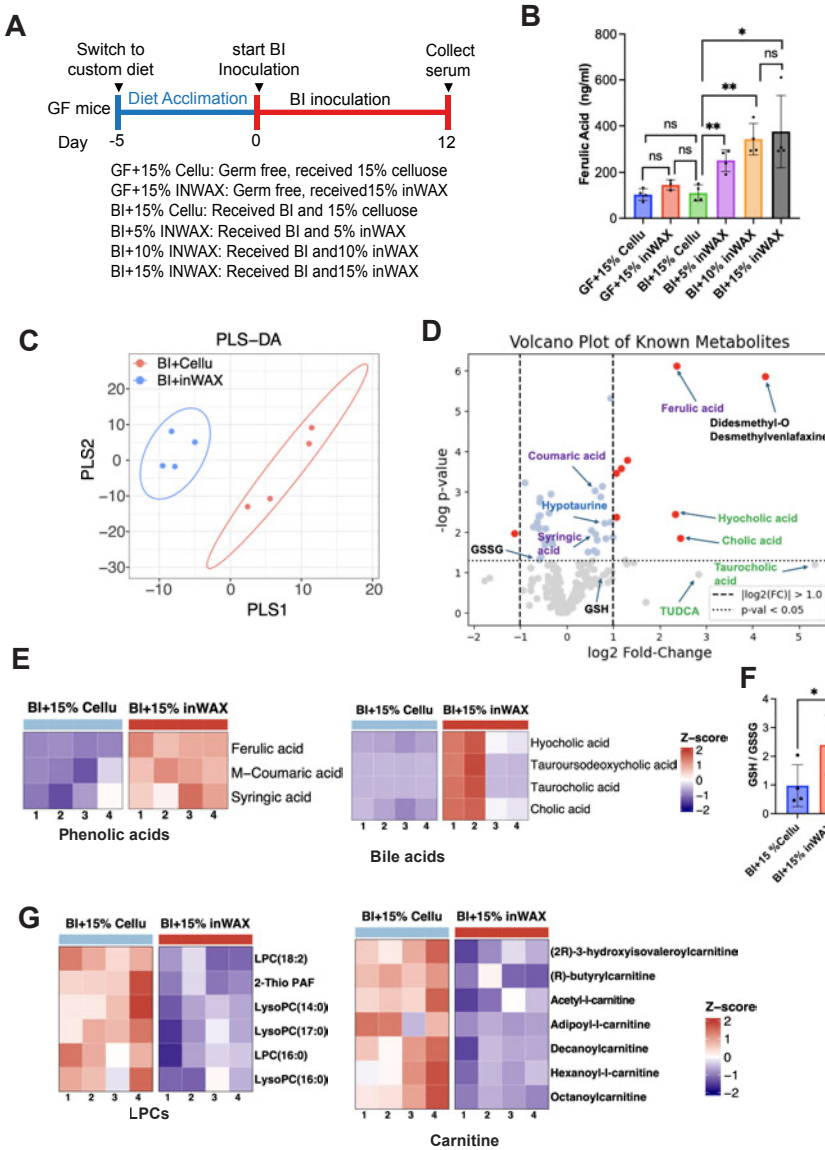
A
Switch to custom diet
start BI Inoculation
Collect serum
GF mice
Diet Acclimation
BI inoculation
Day
-5
0
12
GF+15% Cellu: Germ free, received 15% celluose
GF+15% INWAX: Germ free, received15% inWAX
BI+15% Cellu: Received BI and 15% celluose
BI+5% INWAX: Received BI and 5% inWAX
BI+10% INWAX: Received BI and10% inWAX
BI+15% INWAX: Received BI and15% inWAX
B
Ferulic Acid (ng/ml)
GF+15% Cellu
GF+15% inWAX
BI+15% Cellu
BI+5% inWAX
BI+10% inWAX
BI+15% inWAX
C
PLS-DA
BI+Cellu
BI+inWAX
PLS2
PLS1
D
Volcano Plot of Known Metabolites
Ferulic acid
Didesmethyl-O Desmethylvenlafaxine
Coumaric acid
Hypotaurine
Syringic acid
GSSG
GSH
Hyocholic acid
Cholic acid
Taurocholic acid
TUDCA
|log2(FC)| > 1.0
p-val < 0.05
-log p-value
log2 Fold-Change
E
BI+15% Cellu
BI+15% inWAX
Ferulic acid
M-Coumaric acid
Syringic acid
Phenolic acids
Hyocholic acid
Tauroursodeoxycholic acid
Taurocholic acid
Cholic acid
Bile acids
Z-score
F
GSH / GSSG
BI+15 %Cellu
BI+15% inWAX
G
LPC(18:2)
2-Thio PAF
LysoPC(14:0)
LysoPC(17:0)
LPC(16:0)
LysoPC(16:0)
LPCs
(2R)-3-hydroxyisovaleroylcarnitine
(R)-butyrylcarnitine
Acetyl-l-carnitine
Adipoyl-l-carnitine
Decanoylcarnitine
Hexanoyl-l-carnitine
Octanoylcarnitine
Carnitine

Figure 2

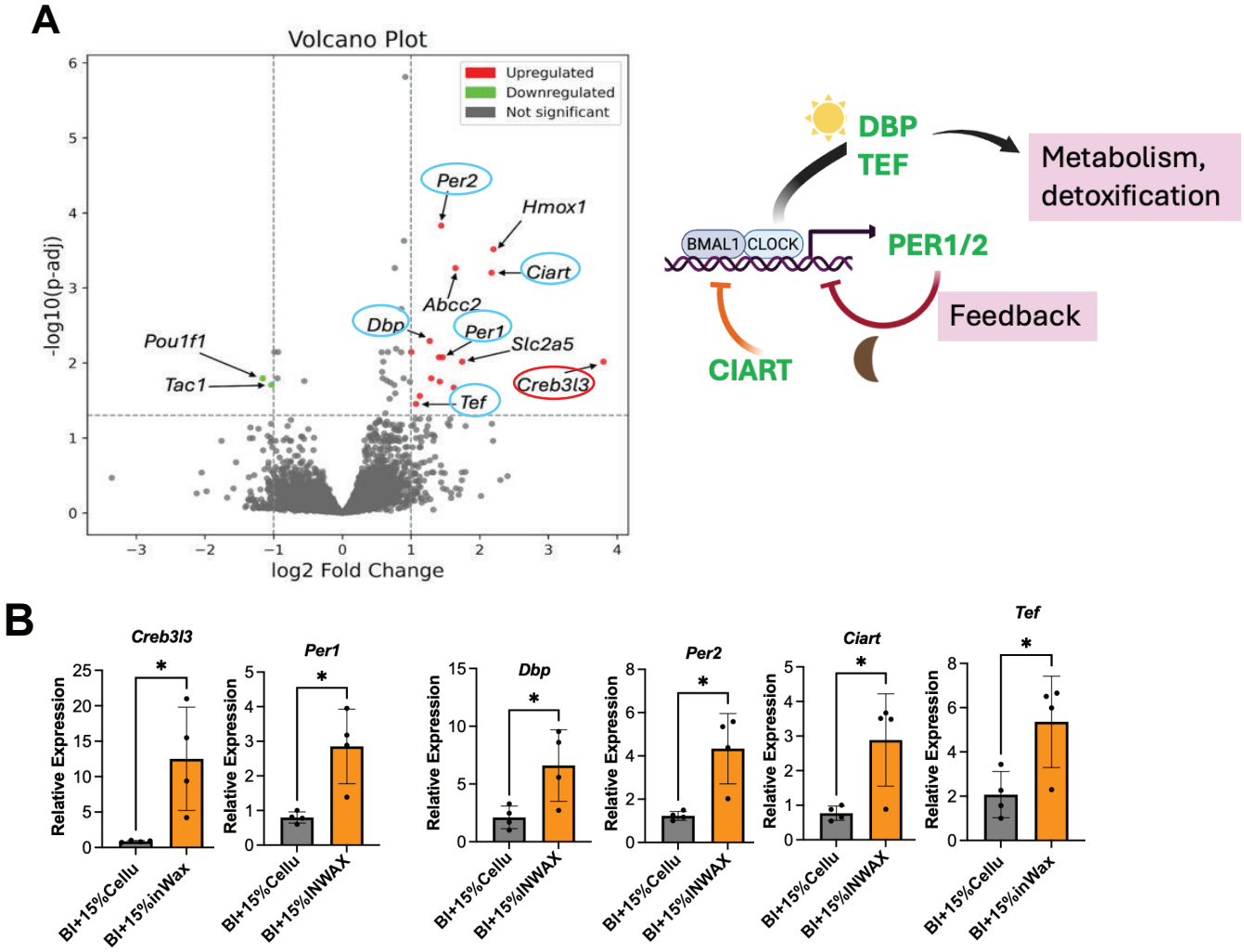
A
Volcano Plot
Upregulated
Downregulated
Not significant
Per2
Hmox1
Ciart
Abcc2
Dbp
Per1
Slc2a5
Pou1f1
Tac1
Creb3l3
Tef
-log10(p-adj)
log2 Fold Change
DBP
TEF
Metabolism, detoxification
BMAL1
CLOCK
PER1/2
Feedback
CIART
B
Creb3l3
Per1
Dbp
Per2
Ciart
Tef
Relative Expression
Bl+15%Cellu
Bl+15%inWax
Bl+15%INWAX

Figure 3

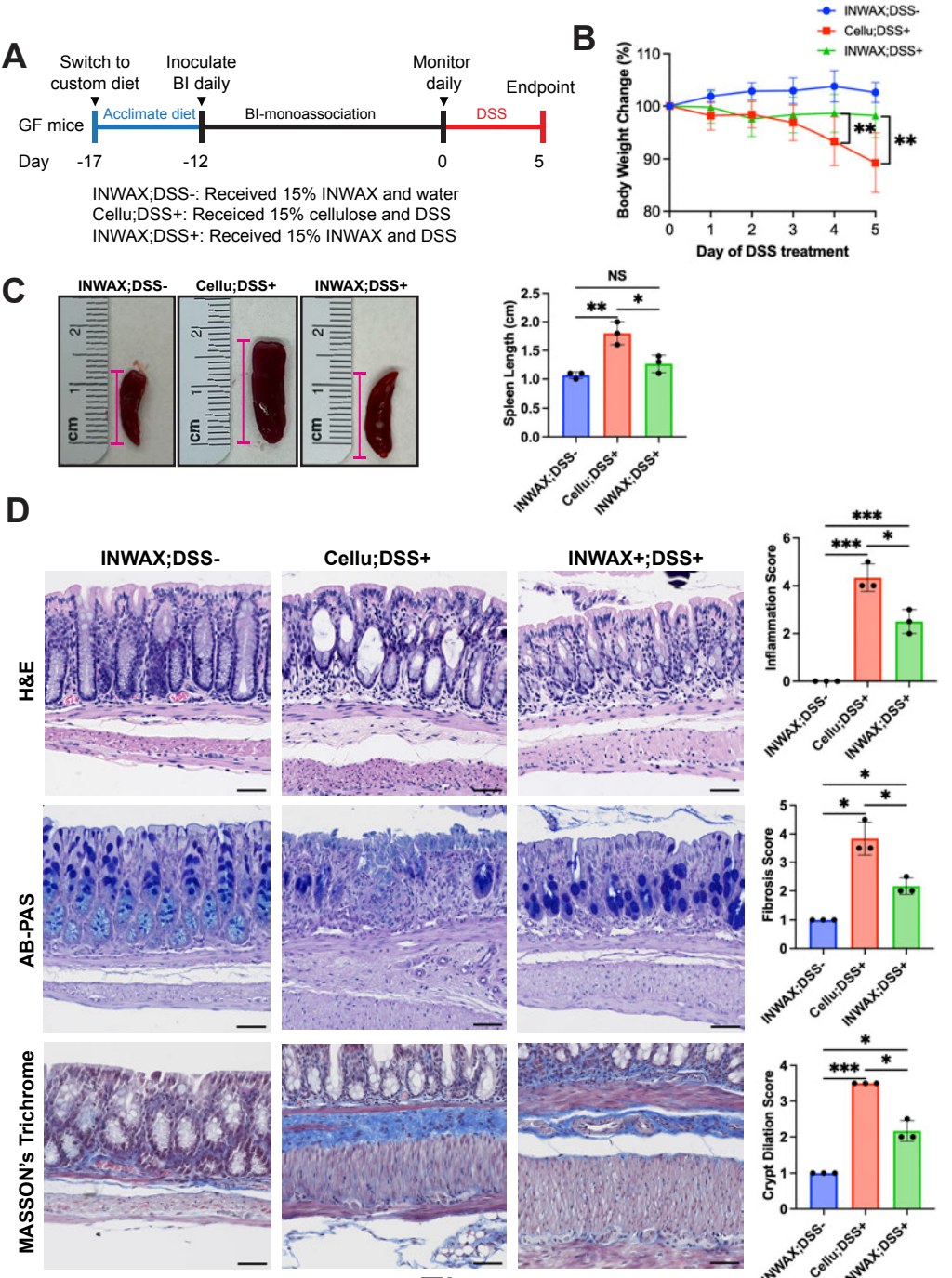
A
Switch to custom diet
Inoculate BI daily
Monitor daily
Endpoint
GF mice
Acclimate diet
BI-monoassociation
DSS
Day
-17
-12
0
5
INWAX;DSS-: Received 15% INWAX and water
Cellu;DSS+: Receiced 15% cellulose and DSS
INWAX;DSS+: Received 15% INWAX and DSS
B
INWAX;DSS-
Cellu;DSS+
INWAX;DSS+
Body Weight Change (%)
Day of DSS treatment
C
INWAX;DSS-
Cellu;DSS+
INWAX;DSS+
Spleen Length (cm)
NS
D
INWAX;DSS-
Cellu;DSS+
INWAX+;DSS+
H&E
AB-PAS
MASSON's Trichrome
Inflammation Score
Fibrosis Score
Crypt Dilation Score

Figure 4

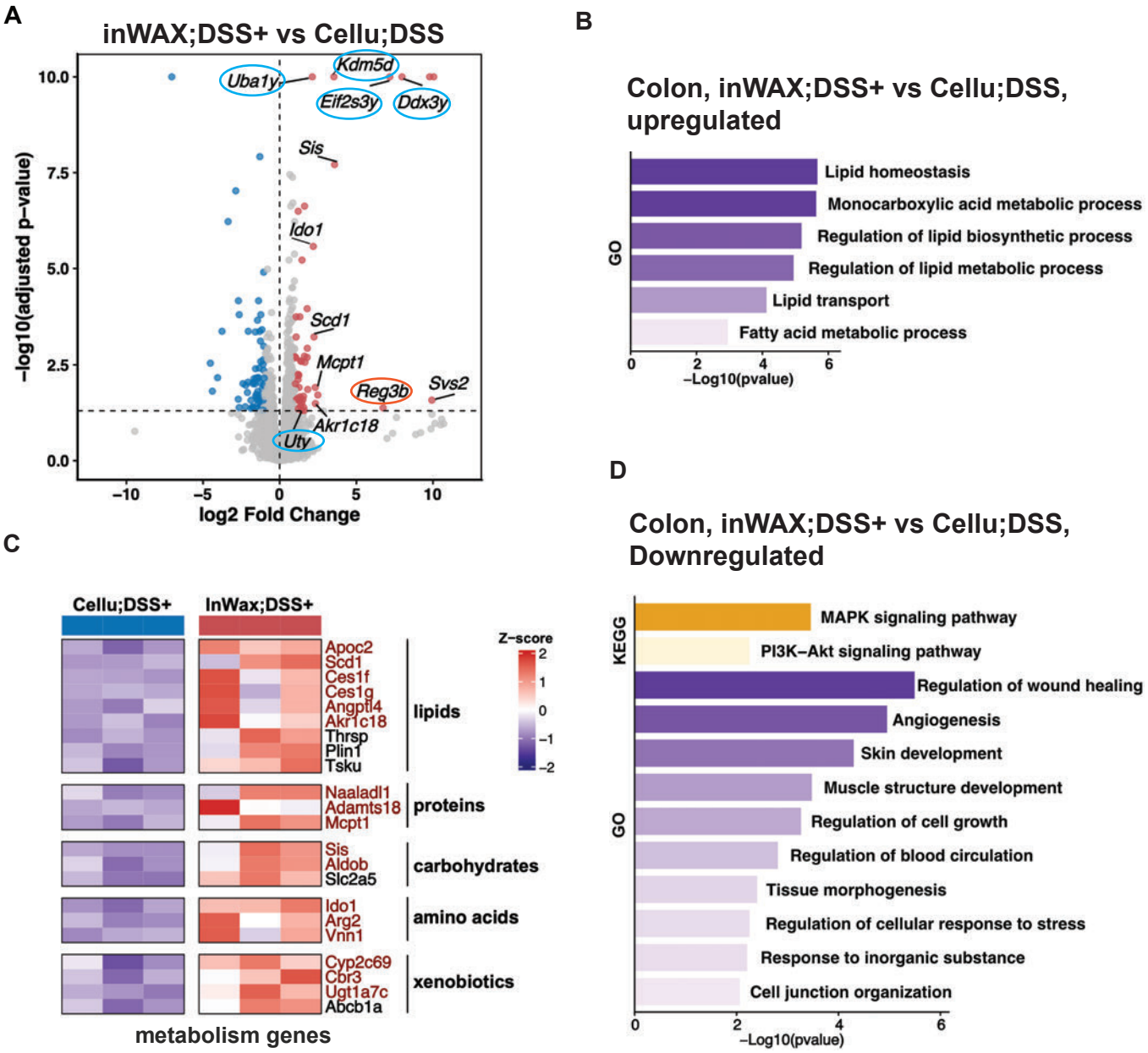
A
inWAX;DSS+ vs Cellu;DSS
Kdm5d
Uba1y
Eif2s3y
Ddx3y
Sis
Ido1
Scd1
Mcpt1
Reg3b
Svs2
Akr1c18
Uty
−log10(adjusted p−value)
log2 Fold Change
B
Colon, inWAX;DSS+ vs Cellu;DSS, upregulated
GO
Lipid homeostasis
Monocarboxylic acid metabolic process
Regulation of lipid biosynthetic process
Regulation of lipid metabolic process
Lipid transport
Fatty acid metabolic process
−Log10(pvalue)
C
Cellu;DSS+
InWax;DSS+
Z−score
Apoc2
Scd1
Ces1f
Ces1g
Angptl4
Akr1c18
Thrsp
Plin1
Tsku
lipids
Naaladl1
Adamts18
Mcpt1
proteins
Sis
Aldob
Slc2a5
carbohydrates
Ido1
Arg2
Vnn1
amino acids
Cyp2c69
Cbr3
Ugt1a7c
Abcb1a
xenobiotics
metabolism genes
D
Colon, inWAX;DSS+ vs Cellu;DSS, Downregulated
KEGG
MAPK signaling pathway
PI3K−Akt signaling pathway
GO
Regulation of wound healing
Angiogenesis
Skin development
Muscle structure development
Regulation of cell growth
Regulation of blood circulation
Tissue morphogenesis
Regulation of cellular response to stress
Response to inorganic substance
Cell junction organization
−Log10(pvalue)

Figure 5

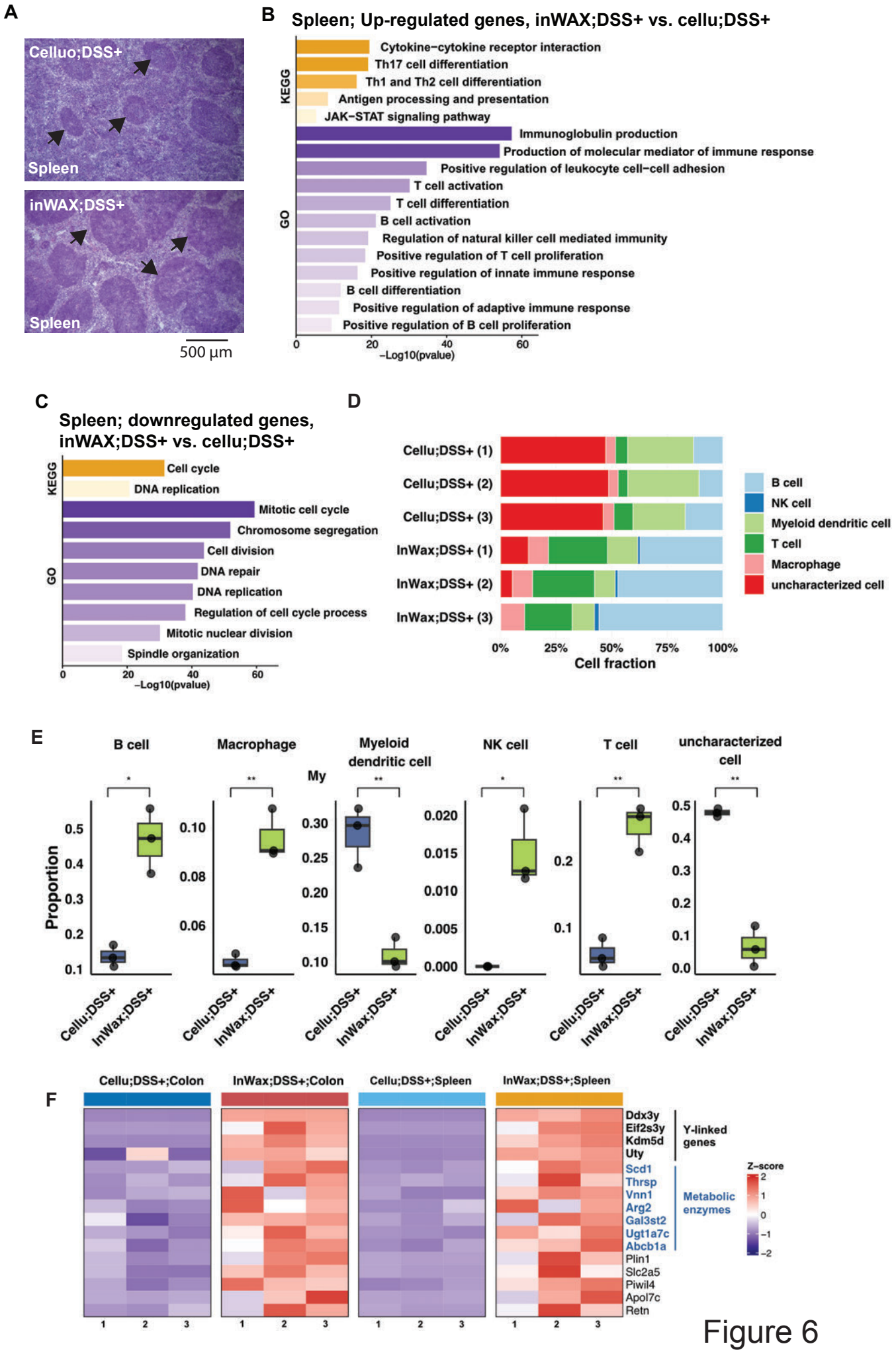
A
Celluo;DSS+
Spleen
inWAX;DSS+
Spleen
500 µm
B
Spleen; Up-regulated genes, inWAX;DSS+ vs. cellu;DSS+
KEGG
Cytokine−cytokine receptor interaction
Th17 cell differentiation
Th1 and Th2 cell differentiation
Antigen processing and presentation
JAK−STAT signaling pathway
GO
Immunoglobulin production
Production of molecular mediator of immune response
Positive regulation of leukocyte cell−cell adhesion
T cell activation
T cell differentiation
B cell activation
Regulation of natural killer cell mediated immunity
Positive regulation of T cell proliferation
Positive regulation of innate immune response
B cell differentiation
Positive regulation of adaptive immune response
Positive regulation of B cell proliferation
0
20
40
60
−Log10(pvalue)
C
Spleen; downregulated genes, inWAX;DSS+ vs. cellu;DSS+
KEGG
Cell cycle
DNA replication
GO
Mitotic cell cycle
Chromosome segregation
Cell division
DNA repair
DNA replication
Regulation of cell cycle process
Mitotic nuclear division
Spindle organization
0
20
40
60
−Log10(pvalue)
D
Cellu;DSS+ (1)
Cellu;DSS+ (2)
Cellu;DSS+ (3)
InWax;DSS+ (1)
InWax;DSS+ (2)
InWax;DSS+ (3)
0%
25%
50%
75%
100%
Cell fraction
B cell
NK cell
Myeloid dendritic cell
T cell
Macrophage
uncharacterized cell
E
B cell
Macrophage
Myeloid dendritic cell
NK cell
T cell
uncharacterized cell
Proportion
Cellu;DSS+
InWax;DSS+
F
Cellu;DSS+;Colon
InWax;DSS+;Colon
Cellu;DSS+;Spleen
InWax;DSS+;Spleen
Ddx3y
Eif2s3y
Kdm5d
Uty
Y-linked genes
Scd1
Thrsp
Vnn1
Arg2
Gal3st2
Ugt1a7c
Abcb1a
Metabolic enzymes
Plin1
Slc2a5
Piwil4
Apol7c
Retn
Z−score
2
1
0
−1
−2
1
2
3

Figure 6

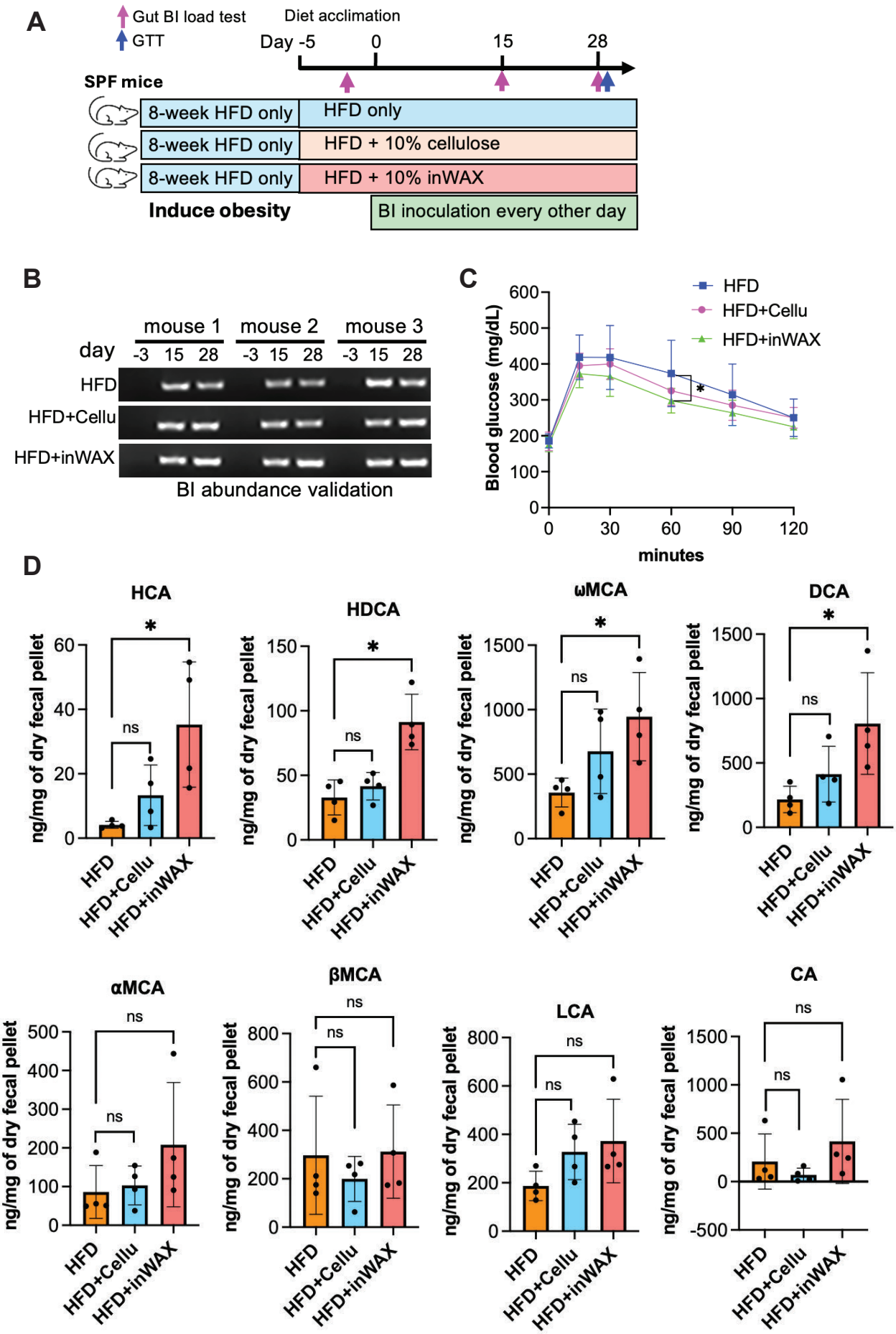
A
Gut BI load test
GTT
Diet acclimation
Day -5
0
15
28
SPF mice
8-week HFD only
HFD only
8-week HFD only
HFD + 10% cellulose
8-week HFD only
HFD + 10% inWAX
Induce obesity
BI inoculation every other day
B
mouse 1
mouse 2
mouse 3
day
-3 15 28
-3 15 28
-3 15 28
HFD
HFD+Cellu
HFD+inWAX
BI abundance validation
C
HFD
HFD+Cellu
HFD+inWAX
Blood glucose (mg/dL)
minutes
D
HCA
HDCA
ωMCA
DCA
αMCA
βMCA
LCA
CA
ng/mg of dry fecal pellet
ns
*
HFD
HFD+Cellu
HFD+inWAX

Figure 7

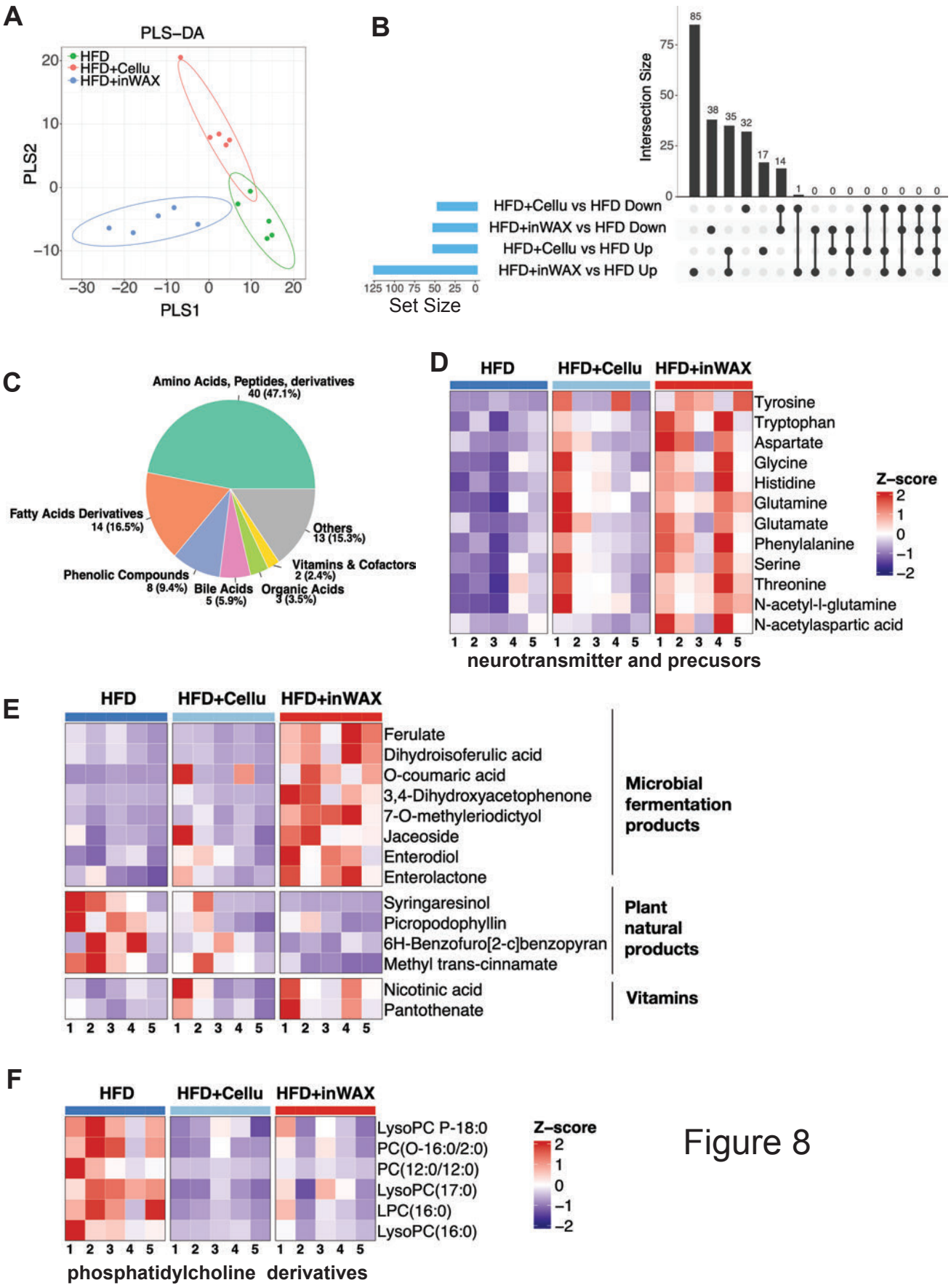
A
PLS–DA
HFD
HFD+Cellu
HFD+inWAX
PLS2
PLS1
B
Intersection Size
85
38
35
32
17
14
1
HFD+Cellu vs HFD Down
HFD+inWAX vs HFD Down
HFD+Cellu vs HFD Up
HFD+inWAX vs HFD Up
Set Size
C
Amino Acids, Peptides, derivatives
40 (47.1%)
Fatty Acids Derivatives
14 (16.5%)
Others
13 (15.3%)
Vitamins & Cofactors
2 (2.4%)
Phenolic Compounds
8 (9.4%)
Bile Acids
5 (5.9%)
Organic Acids
3 (3.5%)
D
HFD
HFD+Cellu
HFD+inWAX
Tyrosine
Tryptophan
Aspartate
Glycine
Histidine
Glutamine
Glutamate
Phenylalanine
Serine
Threonine
N-acetyl-l-glutamine
N-acetylaspartic acid
Z–score
neurotransmitter and precusors
E
HFD
HFD+Cellu
HFD+inWAX
Ferulate
Dihydroisoferulic acid
O-coumaric acid
3,4-Dihydroxyacetophenone
7-O-methyleriodictyol
Jaceoside
Enterodiol
Enterolactone
Microbial fermentation products
Syringaresinol
Picropodophyllin
6H-Benzofuro[2-c]benzopyran
Methyl trans-cinnamate
Plant natural products
Nicotinic acid
Pantothenate
Vitamins
F
HFD
HFD+Cellu
HFD+inWAX
LysoPC P-18:0
PC(O-16:0/2:0)
PC(12:0/12:0)
LysoPC(17:0)
LPC(16:0)
LysoPC(16:0)
Z–score
phosphatidylcholine derivatives

Figure 8